

UNCLASSIFIED

AD NUMBER
AD523538
NEW LIMITATION CHANGE
TO Approved for public release, distribution unlimited
FROM Distribution Controlled. All requests to Dept of the Navy, Office of Naval Research, Attn: Code 421, Arlington, VA 22217
AUTHORITY
ONR ltr dtd 8 Oct 1998

THIS PAGE IS UNCLASSIFIED

UNCLASSIFIED



AD NUMBER

AD-523 538

CLASSIFICATION CHANGES

TO **UNCLASSIFIED**

FROM **CONFIDENTIAL**

AUTHORITY

OCA; DEC 31, 1980

THIS PAGE IS UNCLASSIFIED

AD523538

NR TC 72-10R

**FOURTH QUARTERLY TECHNICAL STATUS REPORT
HIGH POWER CO LASER (U)**

Prepared by
Northrop Research and Technology Center
Laser Technology Laboratories

September 1972

**NO FORM
NOT RELEASABLE TO
FOREIGN NATIONALS**

Contract No. N00014-72-C-0043

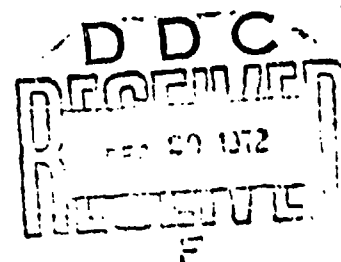
Sponsored by
ADVANCED RESEARCH PROJECTS AGENCY
ARPA ORDER NO. 1806

Monitored by
OFFICE OF NAVAL RESEARCH
CODE 421

This document contains information affecting the National Defense of the United States, within the meaning of the Espionage Laws, Title 18, U.S.C. Sections 793 and 794, the transmission or revelation of which in any manner to an unauthorized person is prohibited by law.

NORTHROP CORPORATION

LASER SYSTEMS DEPARTMENT
3401 West Broadway
Hawthorne, California 90250



DDC CONTROL
22709

NRTC 72-10R

**FOURTH QUARTERLY TECHNICAL STATUS REPORT
HIGH POWER CO LASER (U)**

**Prepared by
Northrop Research and Technology Center
Laser Technology Laboratories**

September 1972

This document contains information affecting the National Defense of the United States, within the meaning of the Espionage Laws, Title 18, U.S.C. Sections 793 and 794, the transmission or revelation of which in any manner to an unauthorized person is prohibited by law.

Contract No. N00014-72-C-0043

**Sponsored by
ADVANCED RESEARCH PROJECTS AGENCY
ARPA ORDER NO. 1806**
26 DEC 1972
Requests

**Monitored by
OFFICE OF NAVAL RESEARCH
CODE 421**

Arlington, Va 22217
N00014-72-C-0043

CLASSIFIED BY DD-254 Nov 72
SUBJECT TO GENERAL DECLASSIFICATION
SCHEDULE OF EXECUTIVE ORDER 11652
AUTOMATICALLY DOWNGRADED AT TWO YEAR
INTERVALS
DECLASSIFIED ON DECEMBER 31, 1980

026 11 1972
22709

**NO FORN
NOT RELEASABLE TO
FORN NATIONALS**

**CNP-2532
Copy 8**



NOTICE

The views and conclusions contained in this document are those of the authors and should not be interpreted as necessarily representing the official policies, either expressed or implied, of the Advanced Research Projects Agency or the U. S. Government.

UNCLASSIFIED

PROGRAM IDENTIFICATION (U)

ARPA Order No. : 1806

Program Code No. : 1E90

Name of Contractor: Northrop Corporation

Effective date of contract: 1 August 1971 - 31 December 1972

Amount of Contract: \$1,331,273.00

Contract No. : N00014-72-C-0043

Program Manager: Dr. G. Hassserjian
(213) 675-4611, Ext 4861

Project Scientist: Dr. M. M. Mann
(213) 675-4611, Ext 2821

Scientific Officer: Director, Physics Program
Physical Sciences Division
Office of Naval Research
Department of Navy
800 North Quincy
Arlington, Virginia 22217

Disclaimer: The views and conclusions contained in this document are those of the authors and should not be interpreted as necessarily representing the official policies, either expressed or implied, of the Advanced Research Projects Agency or the U. S. Government.

UNCLASSIFIED

UNCLASSIFIED

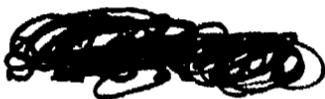
NRTC 72-10R

**FOURTH QUARTERLY TECHNICAL STATUS REPORT
HIGH POWER CO LASER (U)**

TABLE OF CONTENTS (U)

1.0	SUMMARY	1
2.0	PARAMETRIC STUDIES WITH THE KINETIC MODEL	5
	2.1 Comparisons with E-Beam Results	5
	2.2 Sensitivity Tests	12
	2.3 Predictions of the Model	15
3.0	VV CROSS RELAXATION RATE	32
4.0	E-BEAM LASER EXPERIMENTAL RESULTS	42
	4.1 Spectral Data	42
	4.2 Device Development	46
5.0	AREA CATHODE E-GUN DEVELOPMENT	47
	5.1 Experimental Tests	47
	5.2 Theoretical Calculations of Electron Transport Processes	48
	5.3 Primary E-Beam Profile	49
	5.4 Cavity Electric Field	52
	5.5 Cavity Aspect Ratio	54
6.0	REFERENCES	56

UNCLASSIFIED



1.0 SUMMARY

(S) The purpose of this program is to develop, on an approximately 2-3 year time scale, a 1 - 2 MW average power, variable pulse repetition rate diffraction-limited CO laser operating at an electrical efficiency of 50% or more. The work covered in this contract involves the design of intermediate power CO laser devices, the development of the required CO laser technology, and the construction of an intermediate power CO laser device.

(U) This program encompasses, on a best effort basis, the following major tasks:

(U) 1. The development of both steady state and transient kinetic models in order that realistic theoretical predictions of high energy device characteristics can be made.

(U) 2. Measurements of basic parameters of the CO laser at low pressures including: gain, saturation intensity, rates of vibrational cross-relaxation between CO molecules, transfer rates of CO and N₂, discharge characteristics, and spectral characteristics.

(U) 3. Measurements and characterization of a high pressure E-beam excited pulsed laser to experimentally determine transient operating parameters for high energy extraction.

(U) 4. The design and construction of a 500J/pulse diffraction-limited CO laser oscillator.

(U) 6. The development of line selection techniques for controlling the oscillator spectral output.

UNCLASSIFIED

(U) The characterization and modeling investigation of the CO laser kinetics have been quite successful in the last quarter. With extensive experimental data, covering a wide range of parameters, the agreement between our theoretical model and the experimental results appears to be adequate for E-beam stabilized pulsed discharge laser performance predictions. The Jeffers and Kelley VV rate model (with appropriate truncation of the probabilities) coupled with a possible range of optical cross section values show reasonable agreement with cw small signal gain measurements and E-beam pulsed laser output data. Adequate time resolved spectral data are not yet available for comparison with the kinetic model. Data of integrated output spectra obtained to date are also in reasonable agreement with the theory. These results and comparisons with theory are reviewed in Section 2.0 and 3.0. In Section 2.0, using the computer model, performance predictions of pulsed devices at various operating conditions are also described. It is shown that vibrational band selection can be achieved by the appropriate choice of CO partial pressures, electrical pumping rate, and pulse duration (to control temperature rise). The introduction of the characteristics of a water vapor cell (obtained from measured values) in the analytical model shows an effective rotational line selection method. The results with the water vapor cell line selection indicate near 50% efficiency and emission lines having an average attenuation coefficient one half of that of CO₂.

(U) Extensive experimental data were obtained with the E-beam pulsed device (nominal one liter) at various operating conditions. The Northrop constructed E-beam gun, used during the last quarter, is operated at 180 kV and at 40 mA/cm² output current densities. Several problems have been identified in the operation of this laser near liquid nitrogen temperatures

UNCLASSIFIED

UNCLASSIFIED

and pressures above 200 torr. Modifications are currently being made to the device to improve its operation at the low temperature and high pressure regime. A review of the problems, the corrective steps taken and some of the experimental results to date are reviewed in Section 4.0. The table on the next page summarizes the results of the experimentally measured laser output characteristics compared to the objective performance characteristics of a CO pulsed laser. With the modifications being introduced, we anticipate the demonstration of output characteristics closer to the objective values listed in the table.

(U) The construction of the 10 liter device is nearly complete and the testing of the components has been started. The 10 x 100 cm, area cathode E-beam gun has been constructed and tests have begun. A review of the status and the characteristic of the E-gun is given in Section 5.0. In addition, the results of calculations made of electron beam scatter due to the foil and the laser gas are discussed.

UNCLASSIFIED

(U) TABLE I. Experimental Results Versus Objectives - E-Beam Pulsed Device (U)

Parameter	Achieved	Objective
Energy Density	100 - 200 J/l - atm	$\geq 500 \text{ J/l - atm}$
Efficiency - multiline	25 - 40%	$\geq 50\%$
Peak Lasing Bands	$\nu = 8 \rightarrow 7 : 7 \rightarrow 6$	$\leq \nu = 6 \rightarrow 5$
Uniform Medium	300 torr at 150°K	760 torr at 77°K
Pumping Rate	$\leq 8 \text{ kW/cc at } 200 \text{ torr}$	$> 30 \text{ kW/cc at } 760 \text{ torr}$
E-Beam Density	40 mA/cm^2	$> 100 \text{ mA/cm}^2$
Energy Output (1-liter dev)	40 J/pulse	$\geq 100 \text{ J/pulse}$

UNCLASSIFIED

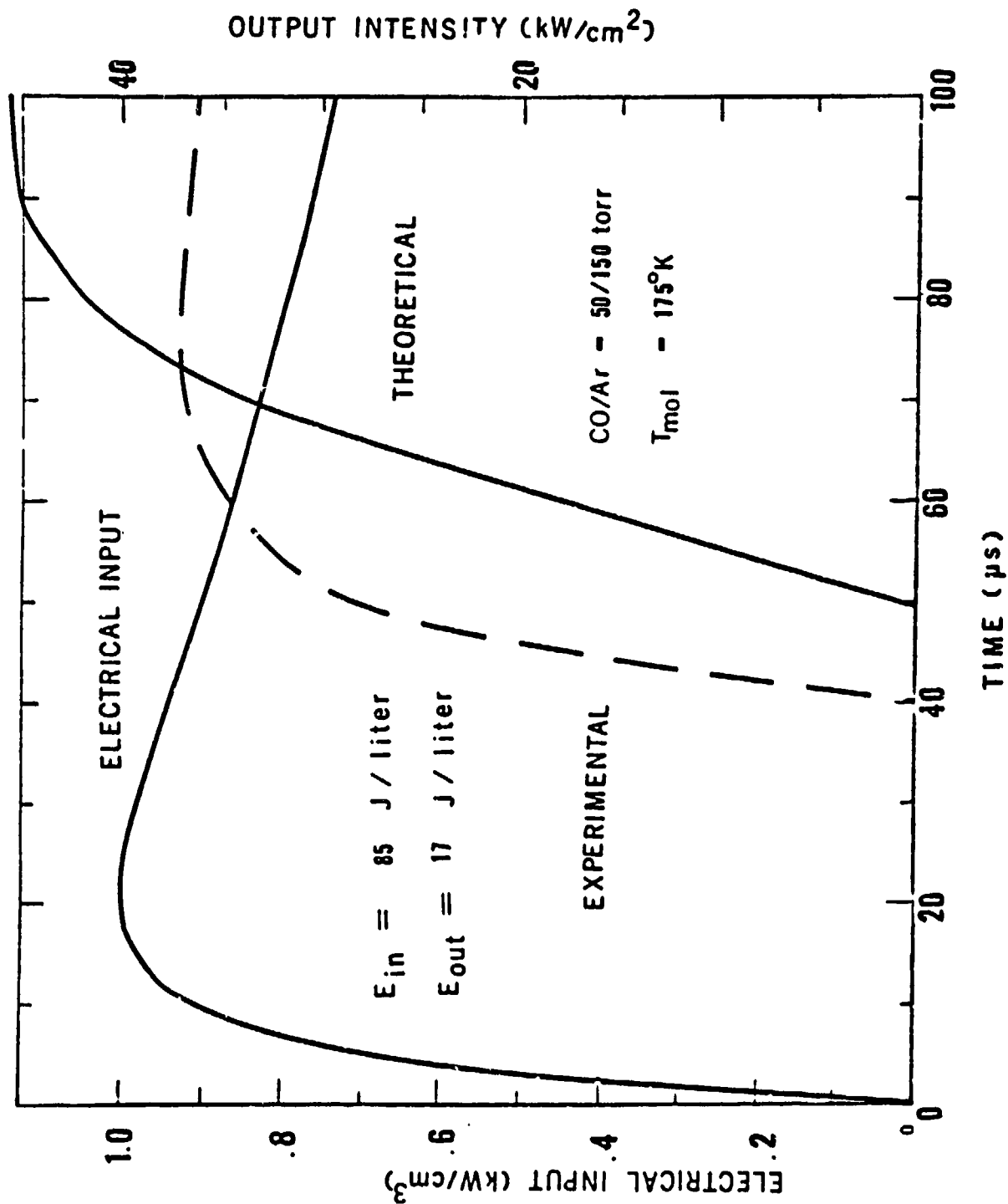
UNCLASSIFIED

2.0 PARAMETRIC STUDIES WITH THE KINETIC MODEL

(U) Recent work in development of the molecular kinetic model now includes a modification in the computer code to allow for kinetic and rotational heating. Using the current version of the model, a variety of calculations have been carried out to compare the theory with experimental data obtained from E-beam laser output, transient gain measurements, and previous small signal gain results. With suitable interpretation, reasonable agreement has been obtained in these comparisons.¹ Furthermore, several assumptions upon which the theory has been based have been modified to test their sensitivity on the predicted output. Calculations for several cases have been carried out, using the currently accepted rate constants, to determine estimated performance for future devices. Finally, sample calculations that include a realistic (but at present nonoptimized) water vapor cell for intracavity line selection are also presented.

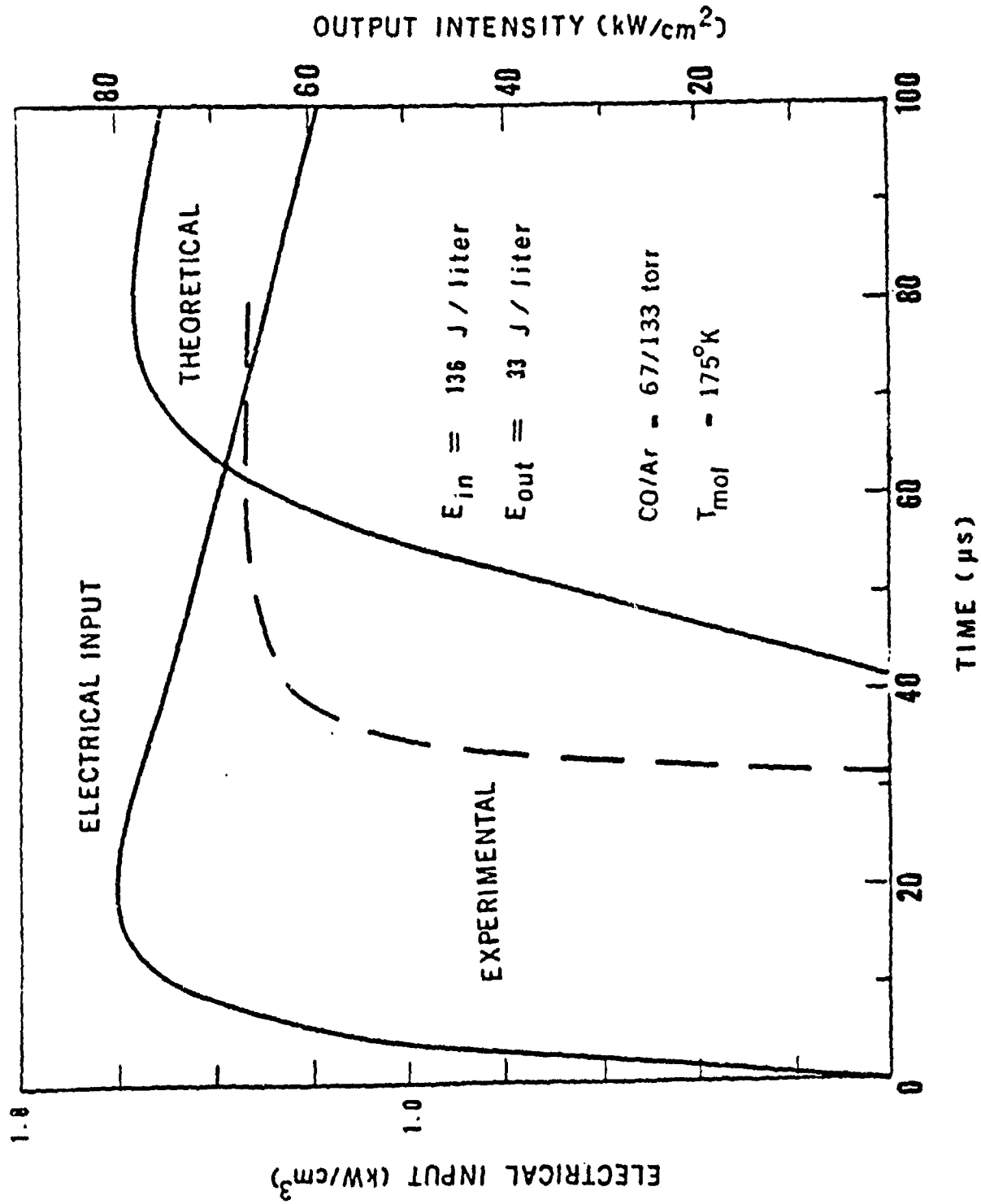
2.1 Comparisons with E-Beam Results. (U) Several cases corresponding to actual E-beam experimental shots have been run under the present version of the kinetic code. Due to the uncertainties in the (CO-N₂) and (N₂-N₂) VV rates, comparisons were limited to gas mixtures containing only CO and Ar. The plasma parameters n_e and T_e were adjusted self-consistently to reproduce the experimentally observed rise and fall times for the electrical input power, as described previously^{1,2}. A variety of gas mixture ratios and excitation powers produced reasonable agreement in the temporal behavior of the output radiation intensities, as shown in Figures 2.1 - 2.6. Since spectral data are presently very limited and difficult to obtain, it is not yet possible to make conclusive comparisons of the time resolved spectral distribution with the theory.

UNCLASSIFIED



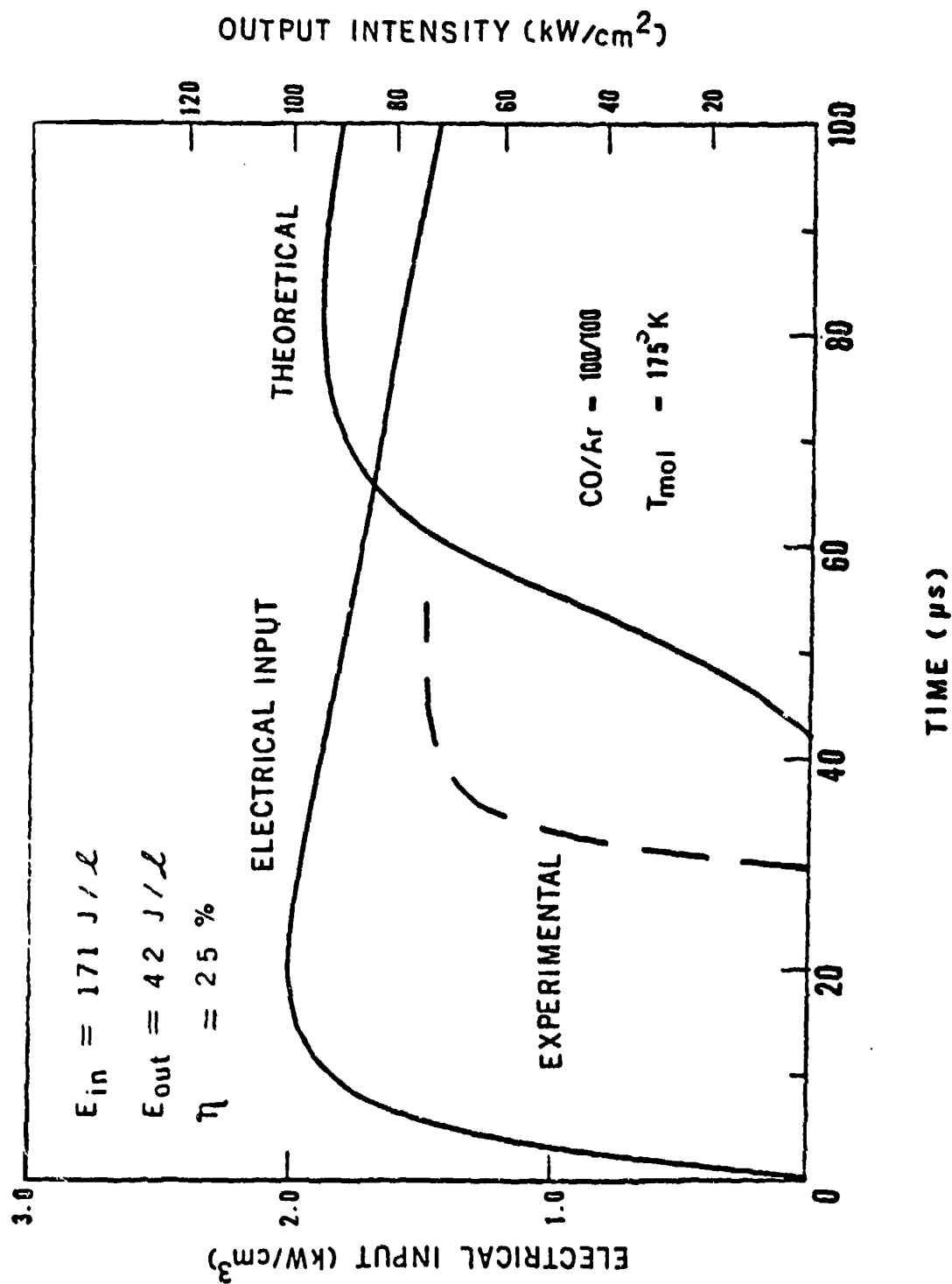
(U) Figure 2.1 Electrical pump power with predicted optical output compared with experimental data from E-beam laser device. (U)

UNCLASSIFIED



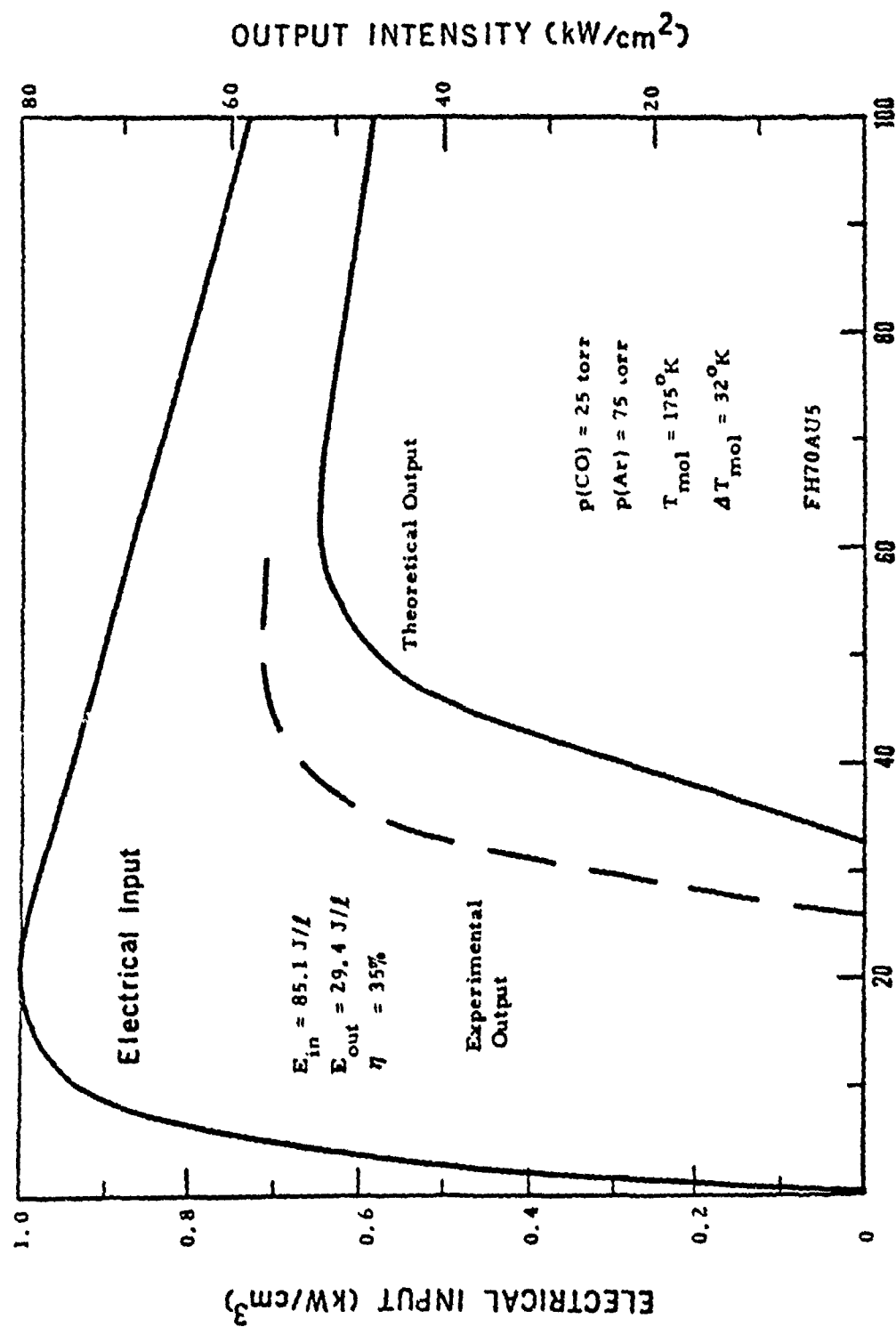
(U) Figure 2.2 Electrical pump power with predicted optical output compared with experimental data from E-beam laser device. (U)

UNCLASSIFIED



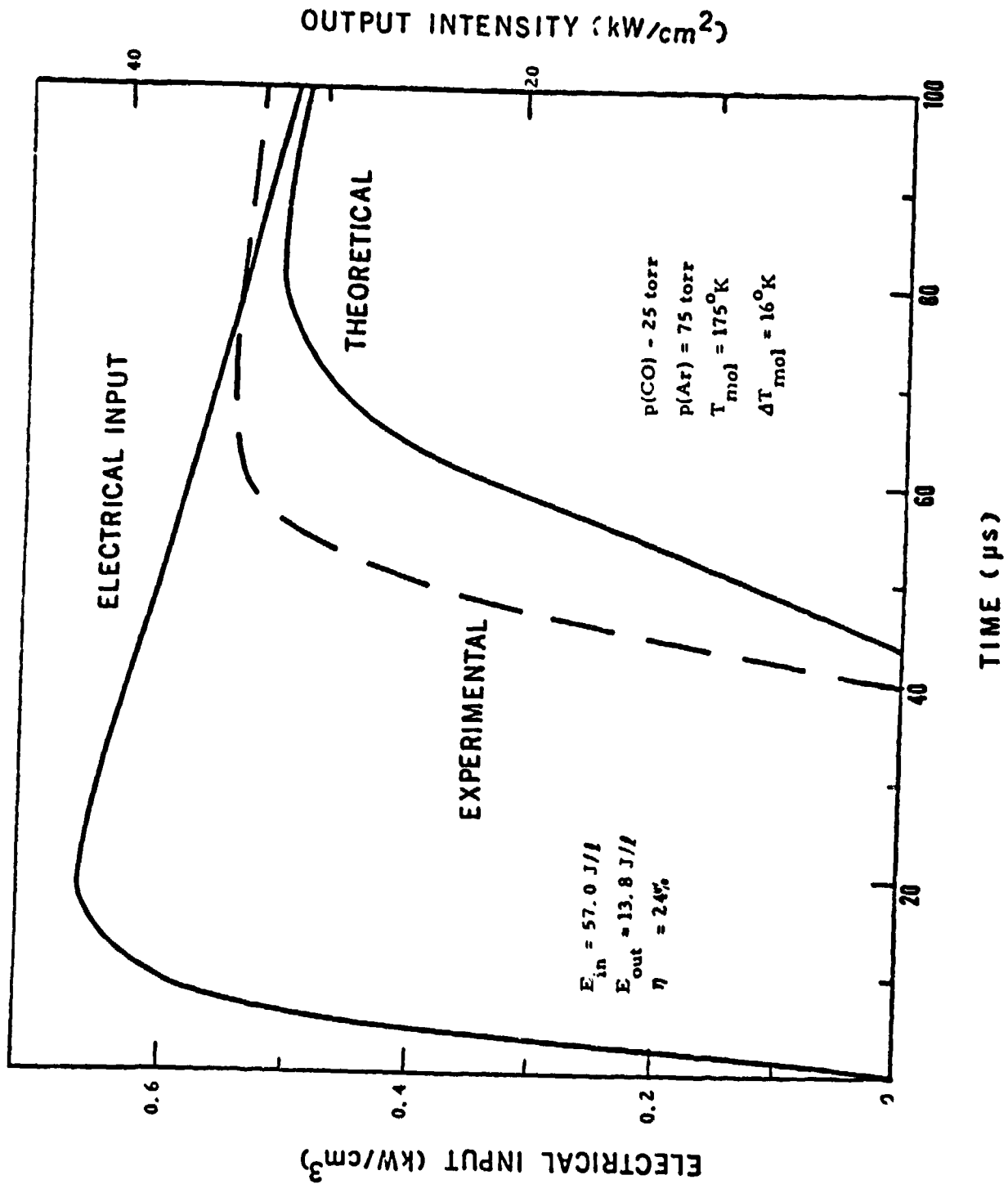
(U) Figure 2.3 Electrical pump power with predicted optical output compared with experimental data from E-beam laser device. (U)

UNCLASSIFIED



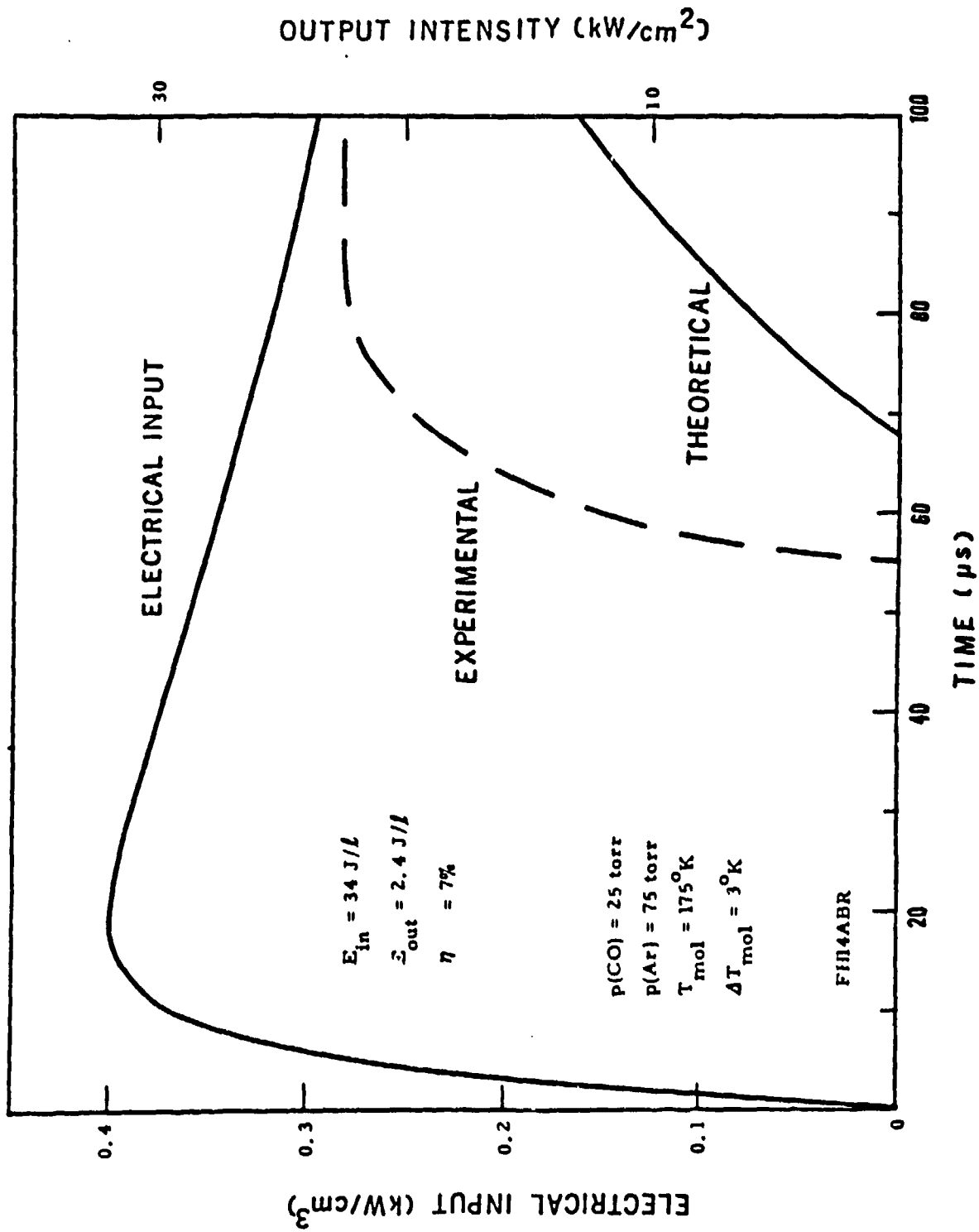
(U) Figure 2.4 Electrical pump power with predicted optical output compared with experimental data from E-beam laser device. (U)

UNCLASSIFIED



(U) Figure 2.5 Electrical pump power with predicted optical output compared with experimental data from E-beam laser device. (U)

UNCLASSIFIED.



(U) Figure 2.6 Electrical pump power with predicted optical output compared with experimental data from E-beam laser device. (U)

UNCLASSIFIED

2.2 Sensitivity Tests. (U) A variety of tests have been made to determine the sensitivity of the model to certain rate constants and input parameters, and predictions have been made of what can be expected from future devices based on the currently accepted rate constants.

(U) Variation of the plasma characteristics showed that detailed predictions of spectral output as a function of time are very insensitive to several different changes, provided that the adjustment of n_e and T_e reproduce the correct input power. Such changes include trade-offs between n_e and T_e , inclusion of excitation processes originating from levels greater than $v = 0$, and actual modification of the Boltzmann assumption. In comparing theory with experiment, the form of the input power as a function of time is known. Thus, because of the insensitivity of the molecular kinetics to the form of the electron distribution, the present approach, which uses a self-consistently adjusted Boltzmann distribution produces very good results.

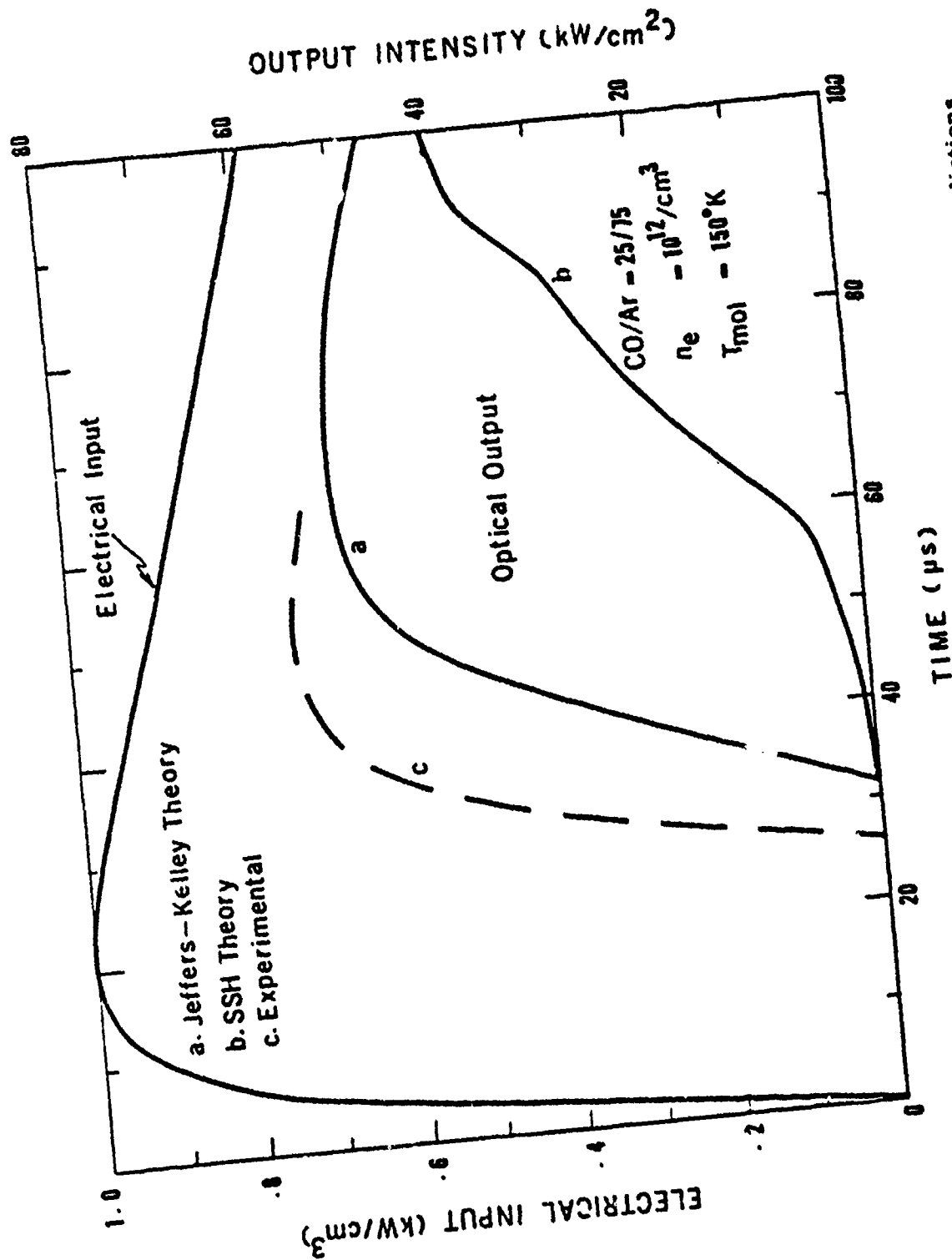
(U) This method is, for example, preferable to using an exact solution obtained at $t = 0$ for $f(E)$, and assuming it to be constant throughout the pulse. Physically, such an approximation can be seen to be inadequate, since the electrical pumping of the vibrational levels raises their vibrational temperatures. Thus, the inelastic vibrational collisions become less effective for limiting the electron energies for a given E/N , and this must be reflected by a change in the distribution as a function of time. Secondly, because of the insensitivity, even an exact time varying solution to the electron Boltzmann equation cannot produce significantly more accurate results for describing the molecular kinetics, and may even be worse if the several approximations required for its solution lead to a result which does not accurately reproduce the temporal input power.

UNCLASSIFIED

(U) Of course, independent plasma calculations for the electron distribution are important and useful for other aspects of the problem. For example, obtaining electron energy balance relations to determine the percentage of total electrical excitation into vibrations, electronic states, ionization, etc., requires the plasma kinetic calculations. They are also necessary for obtaining average electron energies and drift velocities as a function of E/N and gas mixture. Such calculations are important, of course, for estimation of sustainer current, and of values for the parameters n_e and $T_e(0)$ to be used in the kinetic model. The only point of the present discussion is that, if the form of the input power is known, use of a Boltzmann distribution with reasonable values of n_e^0 and $T_e(0)$ and self-consistent adjustment of these quantities as a function of time, provides a very good description of the electrons.

(U) Some tests of the sensitivity to VV rates have also been made, although only a few general conclusions can be drawn from these comparisons at present. Use of the Jeffers-Kelley³ theory as opposed to only a short range SSH theory produced the contrasting results shown in Figure 2.7. It would appear, based on this comparison as well as on the theoretical modeling of the transient gain relaxation data described in Section 3.0, that the long range dipole-dipole contributions of Jeffers-Kelley theory are required for the VV rates. The Jeffers-Kelley theory fits the experimental data of Hancock and Smith at 300°K, but does not agree with low temperature data (100°K) obtained by Wittig and Smith (which seems to suggest that the probabilities are not a sensitive function of temperature). In order to assess this possible defect in the theory, a 150°K case was run using the exothermic Jeffers-Kelley probabilities corresponding to 300°K, but retaining the factors for detailed balance at 150°K to obtain the endothermic rates. This did not produce significant changes in the radiative predictions from the molecular kinetic model.

UNCLASSIFIED



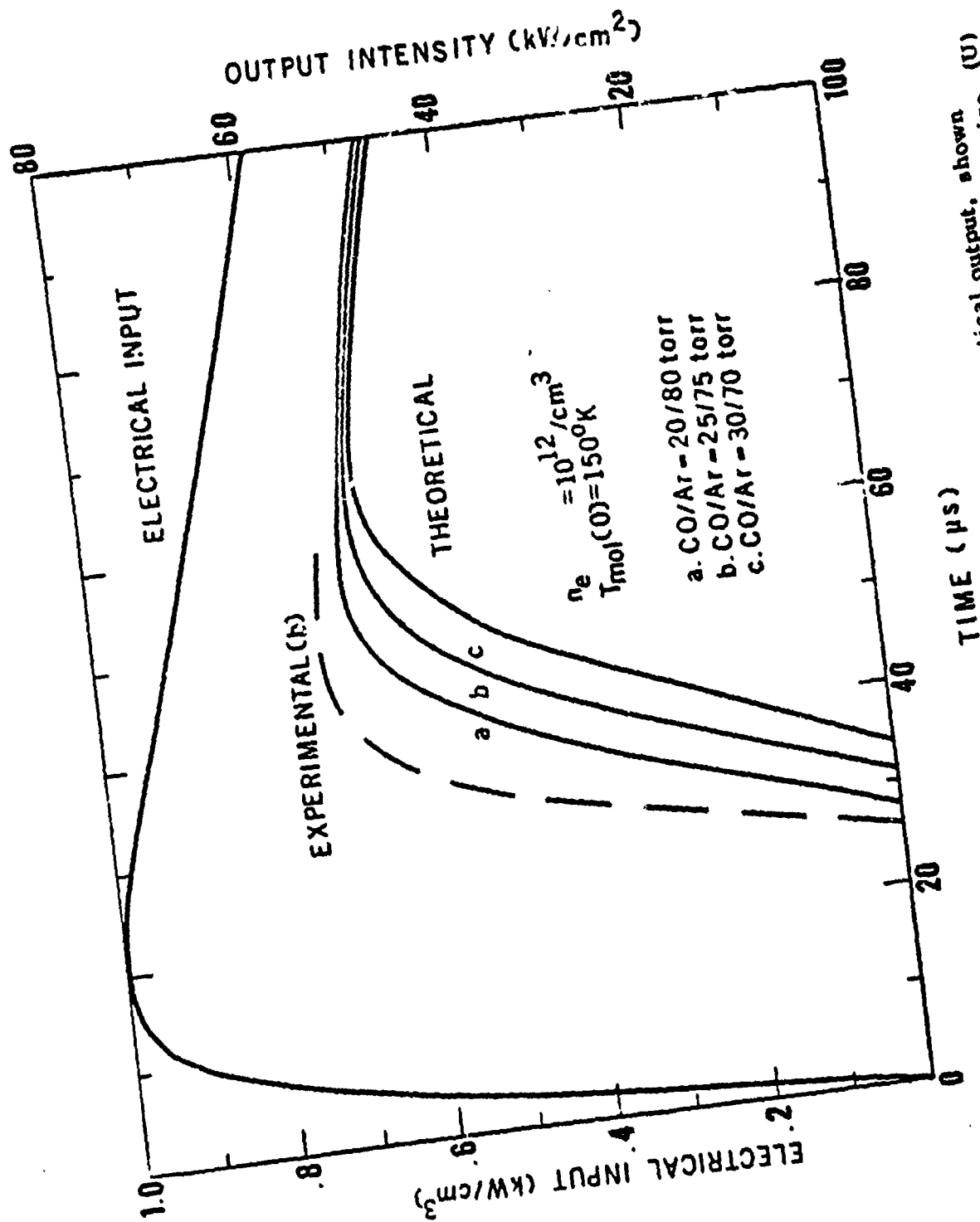
(U) Figure 2.7 Data of Figure 2.4 is reproduced to show contrasting predictions of Jeffers-Kelley theory and SSH theory. (U)

UNCLASSIFIED

(U) The effects of pressure are illustrated in Figure 2.8, for three different cases corresponding to a fixed electrical input power. The effects of electrical input power for a fixed gas mixture are shown in Figure 2.9, which is simply a combination of Figures 2.4 - 2.6 to show the comparison. Note the earlier turn-on times and higher output intensities for increased electrical excitation.

2.3 Predictions of the Model. (U) Figure 2.10 and 2.11 present results for a 1/2 atm and a 1 atm case respectively, with different pumping rates illustrated in Figure 2.11. In Figure 2.10, the effects of different rise times are illustrated, along with display of the increase in kinetic temperature rise as a function of time. For a 20 μ sec pulse, the energy and efficiency results for Figure 2.11 are summarized in Table II. The atmospheric case was used to make comparisons between a free-running and a line selected oscillator. The water vapor cell was assumed to contain 400 torr of H_2O at 420°K, with a path length of 71 cm. Power transfer percentage curves which illustrate the comparison are presented in Figure 2.12. Note the effect that the additional absorption presented by the water vapor cell has on energy output and efficiency, and also the more erratic time dependence of the optical output, which is a reflection of the fact that the losses are frequency dependent and the spectrum is changing through the pulse. The output spectra as a function of time for the two cases are shown in Figure 2.13 for the first six bands. Note the "clamping" effect that the line-selected oscillator exhibits, in contrast to the steady spectral evolution displayed by the free running oscillator. These cases are presented only as examples, and do not represent an optimum choice of parameters. However, they do illustrate the necessity for pumping at a much lower rate to minimize the temporal heating during the pulse.

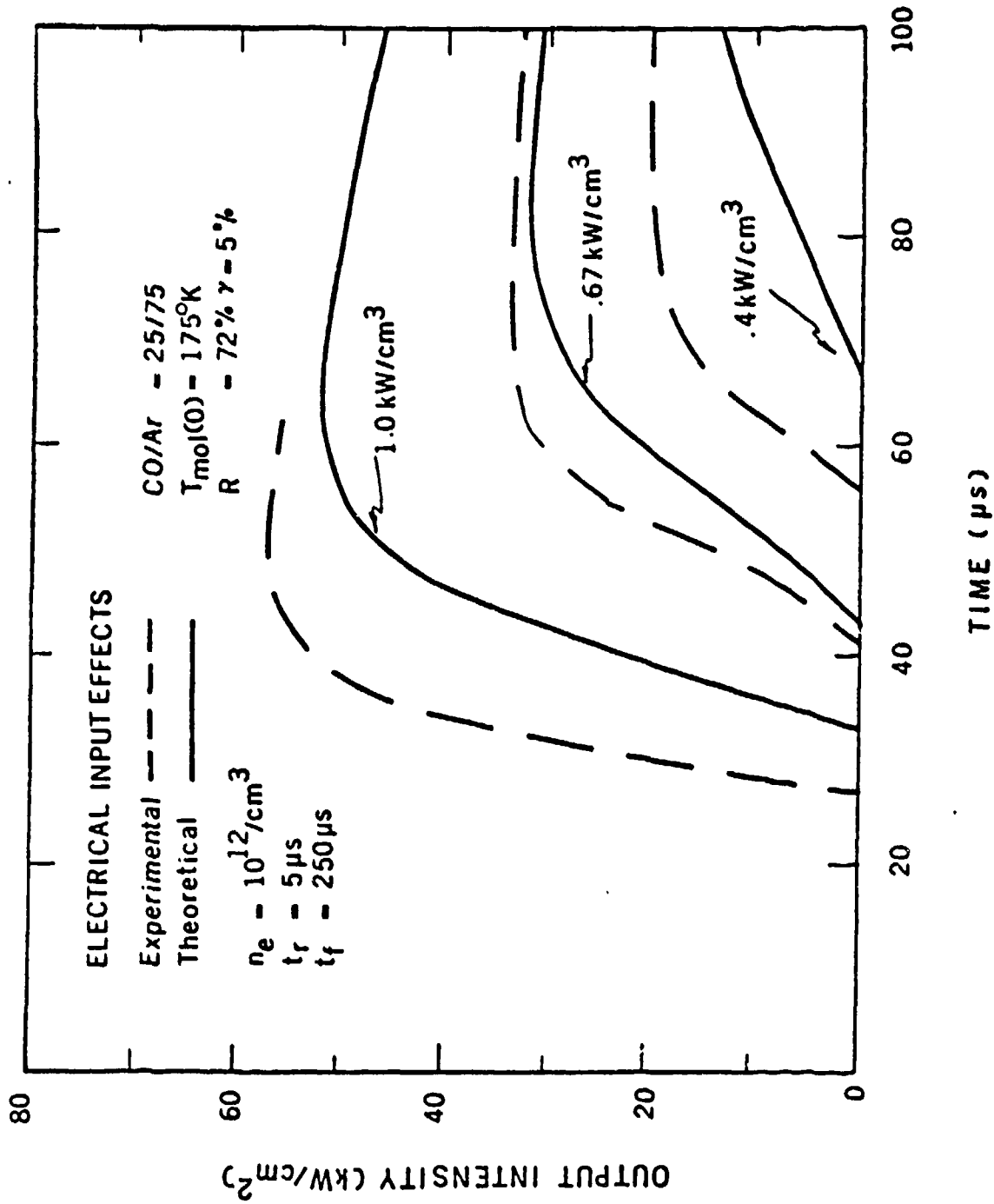
UNCLASSIFIED



(U) Figure 2.8 Effects of pressure variation on predicted optical output, shown compared with data of (b) obtained from the E-beam laser device. (U)

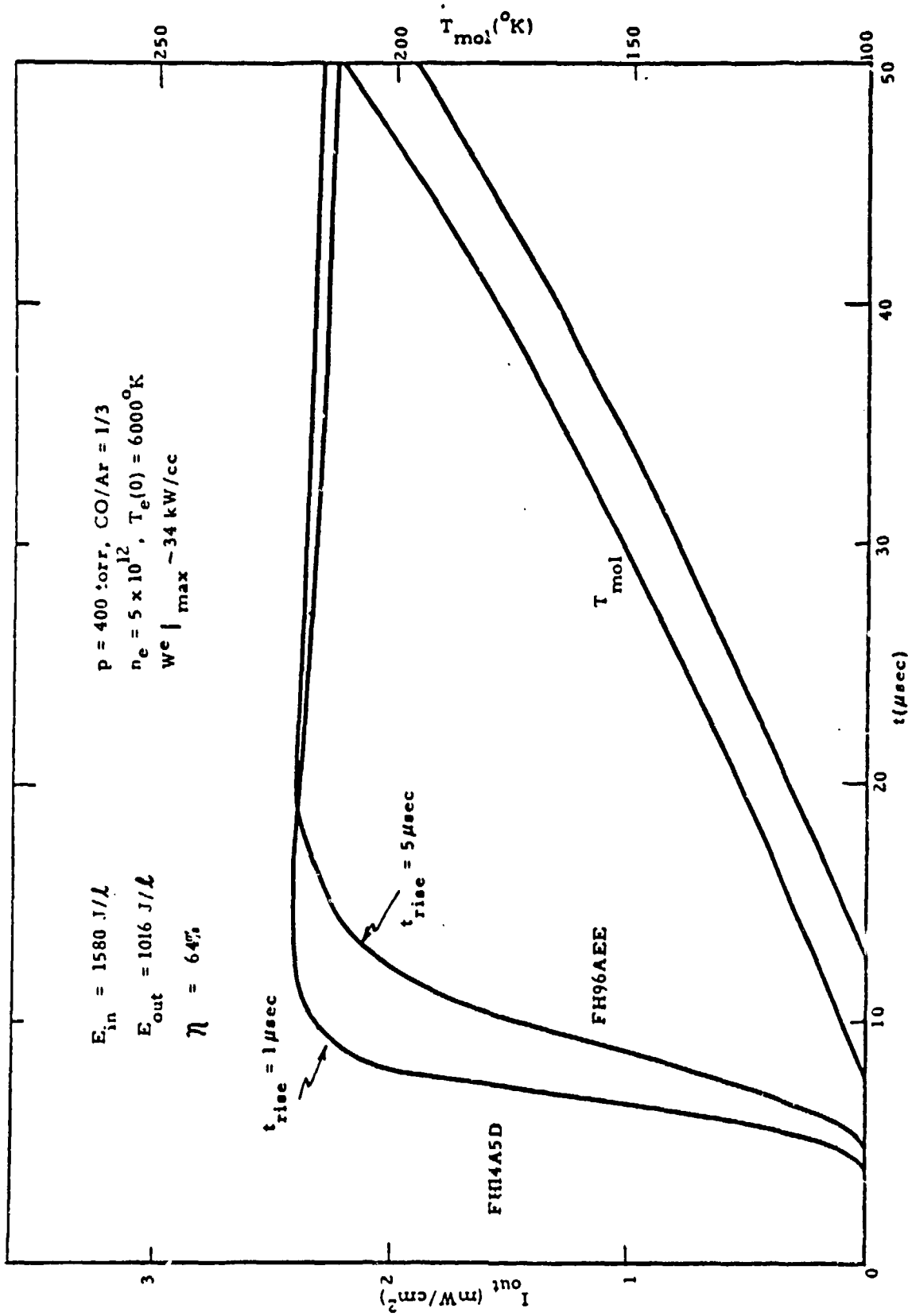
UNCLASSIFIED

UNCLASSIFIED



(U) Figure 2.9 Effects of electrical pumping power on optical output intensity, compared with experimental data from the E-beam laser device (Figures 2.4 - 2.6 have been combined to show comparison). (U)

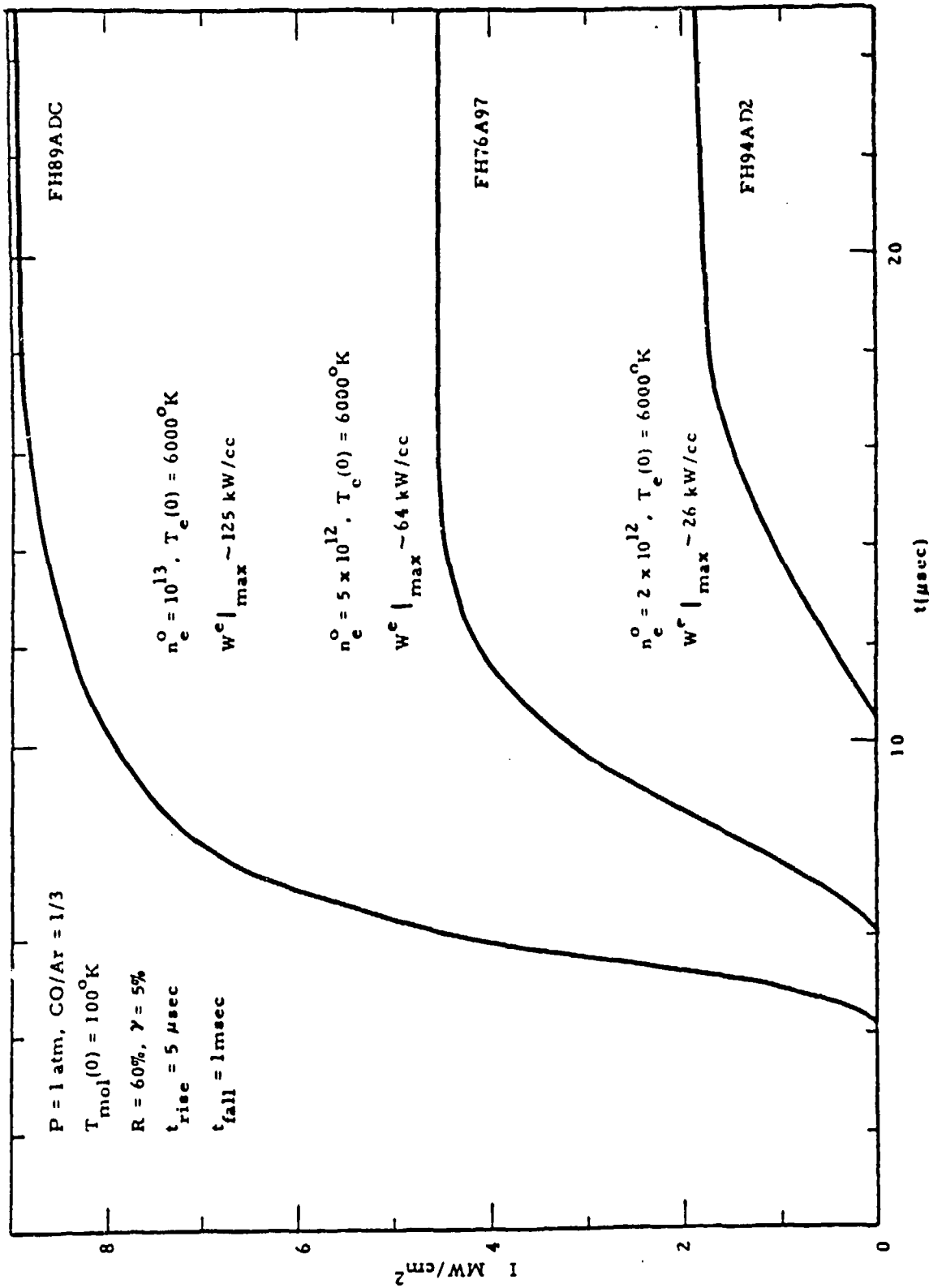
UNCLASSIFIED



(U) Figure 2.10 Total output intensity and kinetic temperature as a function of time for a half-atmosphere oscillator pumped at $\sim 34 \text{ kW/cm}^2$. Effects of electrical input power rise time are also illustrated. (11)

UNCLASSIFIED

UNCLASSIFIED



(U) Figure 2.11 Total output intensity as a function of time for an atmospheric pressure pulsed oscillator, illustrating effects of increased electrical pumping. (U)

UNCLASSIFIED

UNCLASSIFIED

(U) TABLE II. Parameters for Figure 2.11. (U)

20 μ SEC PULSE

● 125 kW/cc

$$E_{in} = 1950 \text{ J/l}$$

$$E_{out} = 1176 \text{ J/l}$$

$$\eta = 60\%$$

$$\Delta T_{mol} = 57^{\circ}\text{K}$$

● 64 kW/cc

$$E_{in} = 953 \text{ J/l}$$

$$E_{out} = 493 \text{ J/l}$$

$$\eta = 52\%$$

$$\Delta T_{mol} = 19^{\circ}\text{K}$$

● 26 kW/cc

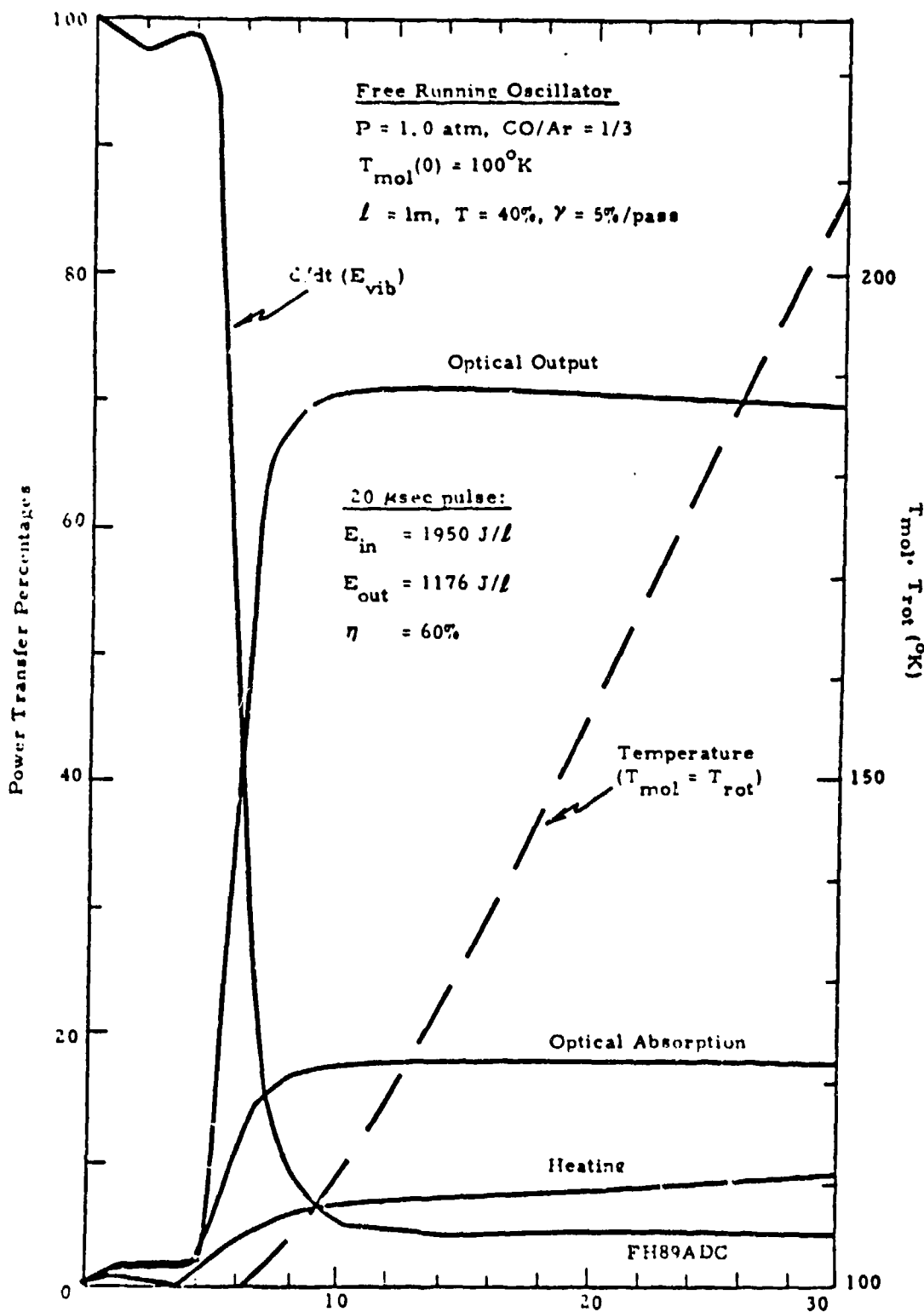
$$E_{in} = 390 \text{ J/l}$$

$$E_{out} = 114 \text{ J/l}$$

$$\eta = 29\%$$

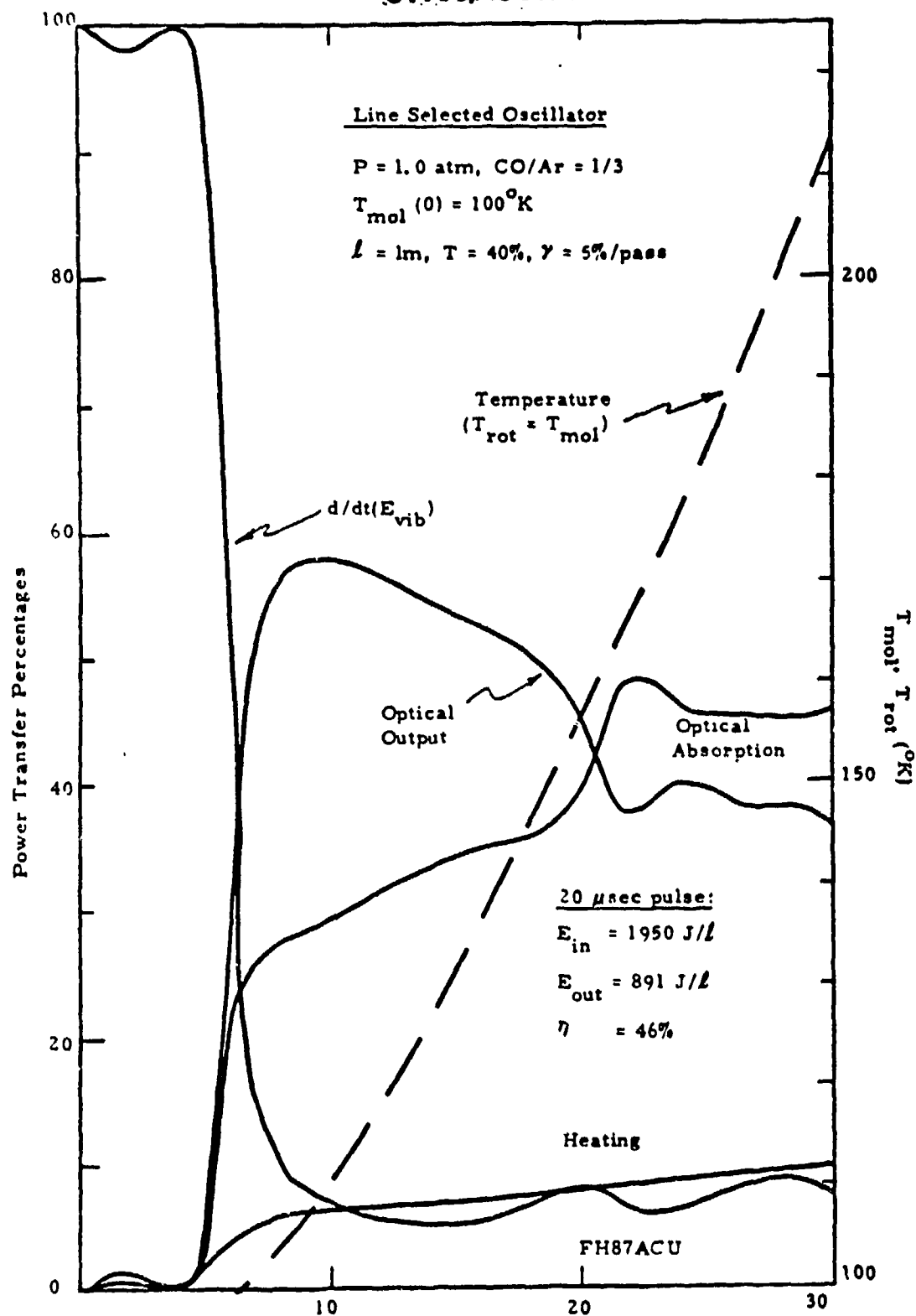
$$\Delta T_{mol} = 5^{\circ}\text{K}$$

UNCLASSIFIED



(U) Figure 2.12a Percentage of electrical power transferred to all mechanisms as a function of time for an atmospheric pressure, pulsed oscillator. (U)

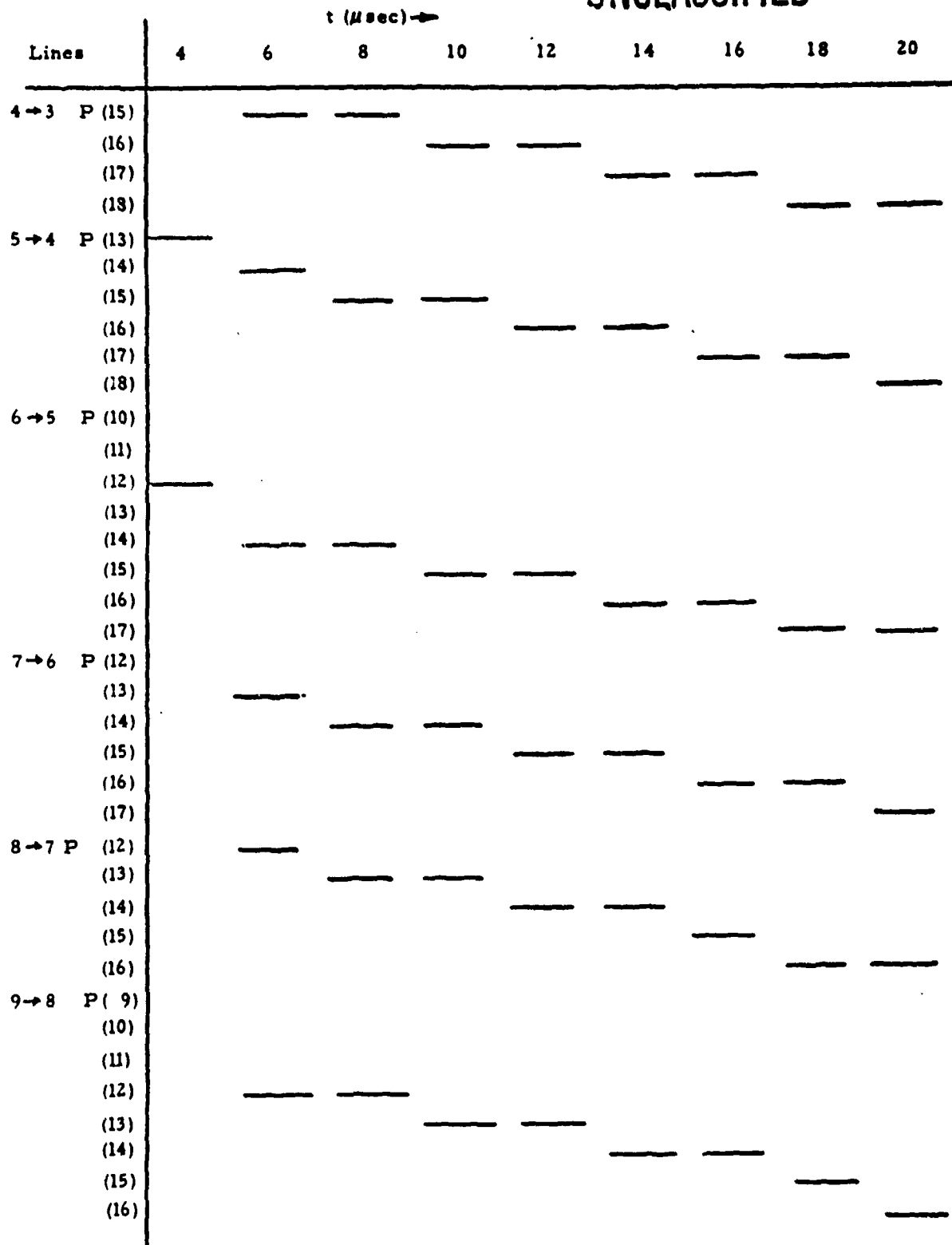
UNCLASSIFIED



(U) Figure 2.12b Percentage of electrical power transferred to all mechanisms as a function of time for a line selected oscillator (intracavity cell containing 400 torr of H_2O at 420°K). (U)

FREE RUNNING OSCILLATOR

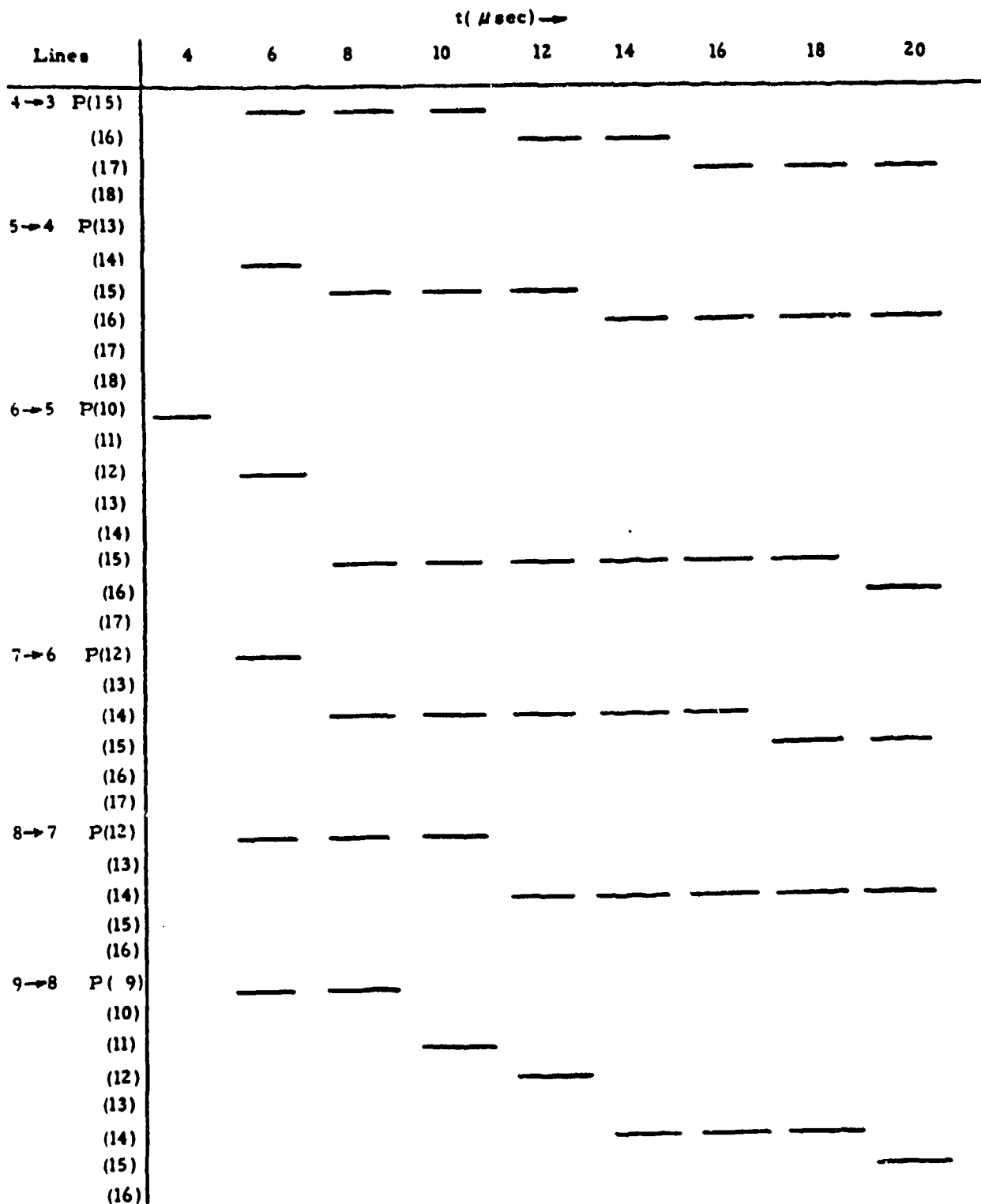
UNCLASSIFIED



(U) Figure 2. 13a Free running oscillator spectral output of Figure 2. 12a. (U)

UNCLASSIFIED

LINE SELECTED OSCILLATOR



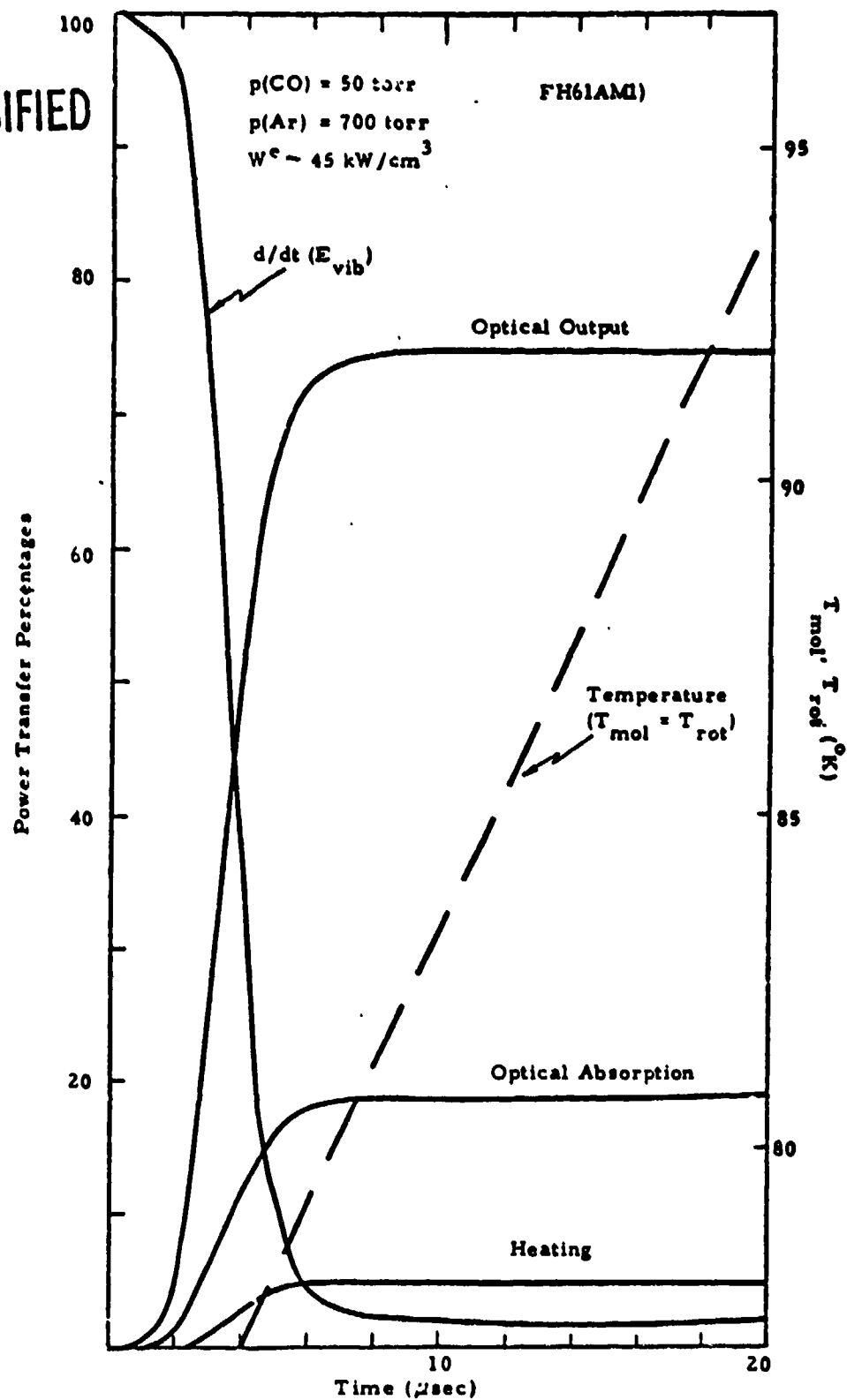
(U) Figure 2. 13b Line selected oscillator spectral output of Figure 2. 12b. (U)

UNCLASSIFIED

(U) A realistic device will require much lower partial pressures of CO to obtain a lower v-band spectral output, and more moderate pumping rates to insure that the spectrum is reasonably constant over most of the pulse duration. Two further examples of free running and line selected oscillators at 77°K are presented to illustrate how certain desirable characteristics can be achieved. The line selection was produced with a 71 cm intracavity cell containing 500 torr H₂O at 420°K. Output coupling was assumed to be provided by a 60% reflecting mirror, with a cavity containing an additional 5%/pass loss over a total gain length of 1 meter.

(U) Figure 2.14 and 2.15 summarize the operating conditions assumed and the transient power transfer percentages for the two cases. As is apparent from both of these figures, steady state is attained after a few microseconds. When an intracavity water vapor cell is introduced into the calculation, the ratio between output coupling and absorption decreases. Temperature rises are modest for pulse lengths 20 - 50 μs under these conditions. Output spectra are presented which illustrate the line selective properties of the water vapor cell, as contrasted to free-running oscillators, in Figure 2.16 and 2.17. Note that the output spectrum is reasonably constant over the pulse length for Figure 2.17b and that the lines respond to those whose atmospheric transmission characteristics are reasonably good. Calculations based on the selection of a single line (4 → 3 P(8)) using an extra loss of 20% round trip (e.g., from a grating) with the same conditions of Figure 2.17 resulted in poor energy efficiency (~15% for a 30 μs pulse). However, it should be noted that the assumed 20% loss of the grating is in the oscillator only, and thus would not preclude the possibility of attaining higher output conversion efficiencies in a MOPA arrangement.

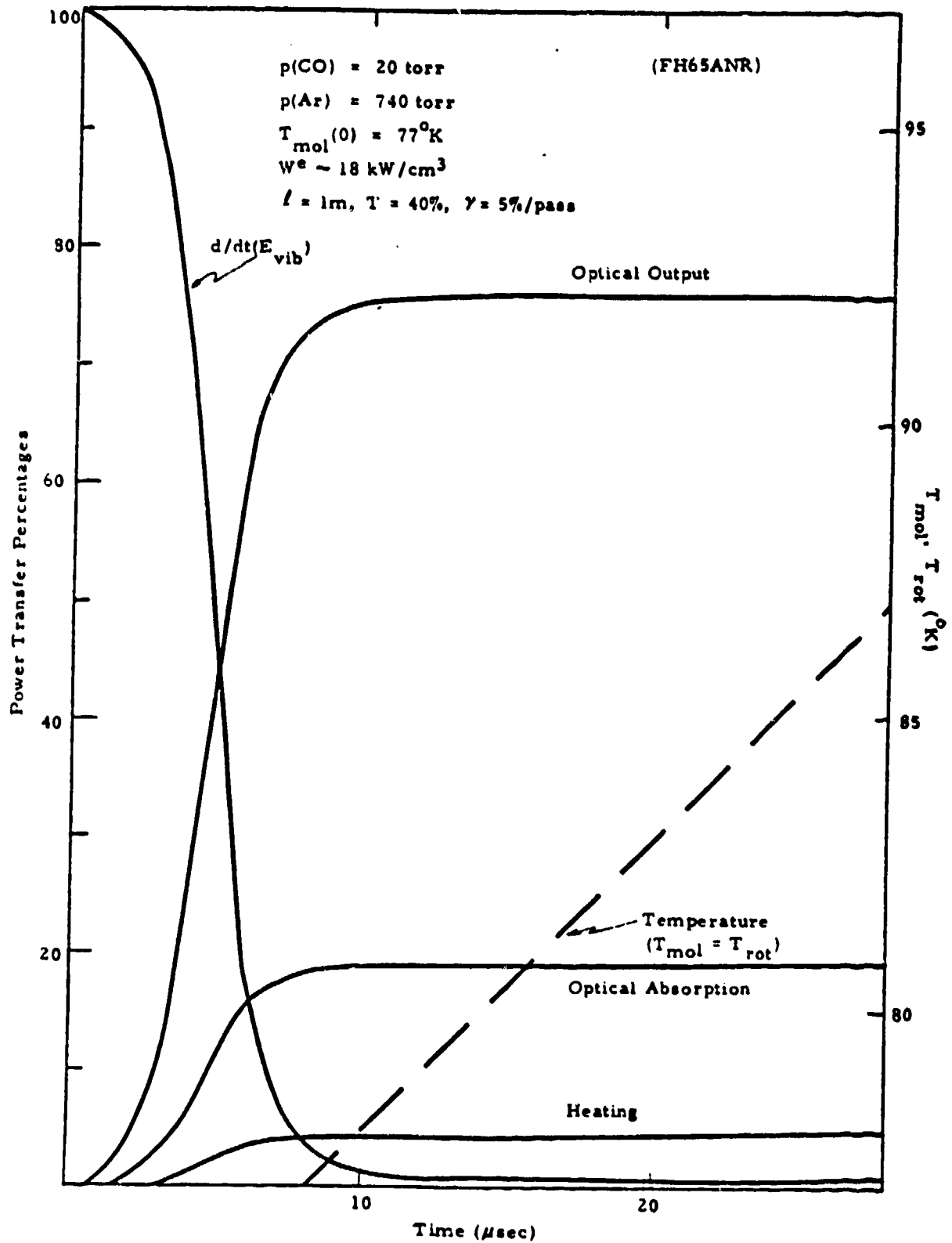
UNCLASSIFIED



(U) Figure 2.14 Percentage of electrical input power transferred into all mechanisms for an atmospheric pressure oscillator. (U)

UNCLASSIFIED

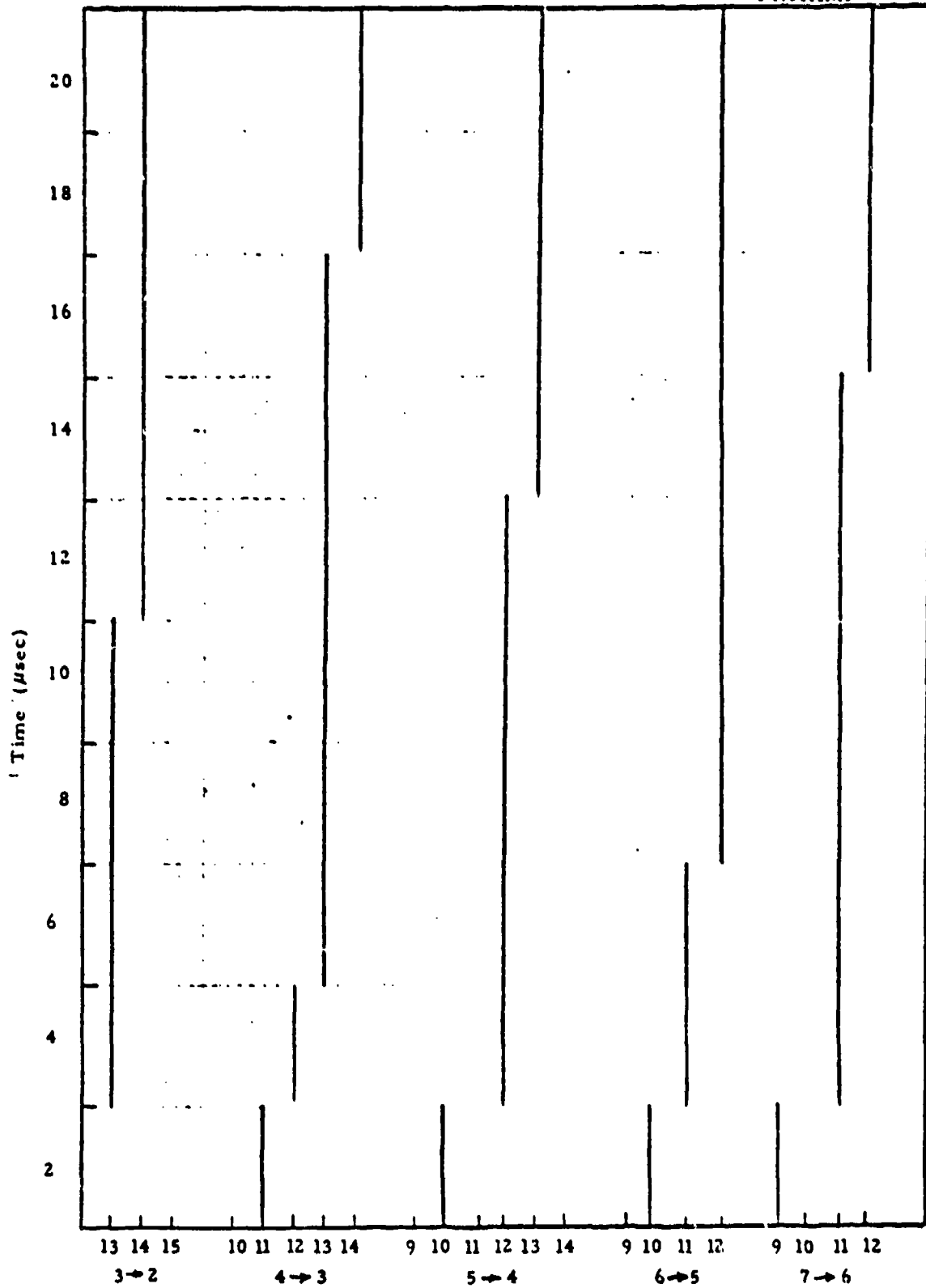
UNCLASSIFIED



(U) Figure 2.15 Percentage of electrical input power transferred into all mechanisms for an atmospheric pressure oscillator. (U)

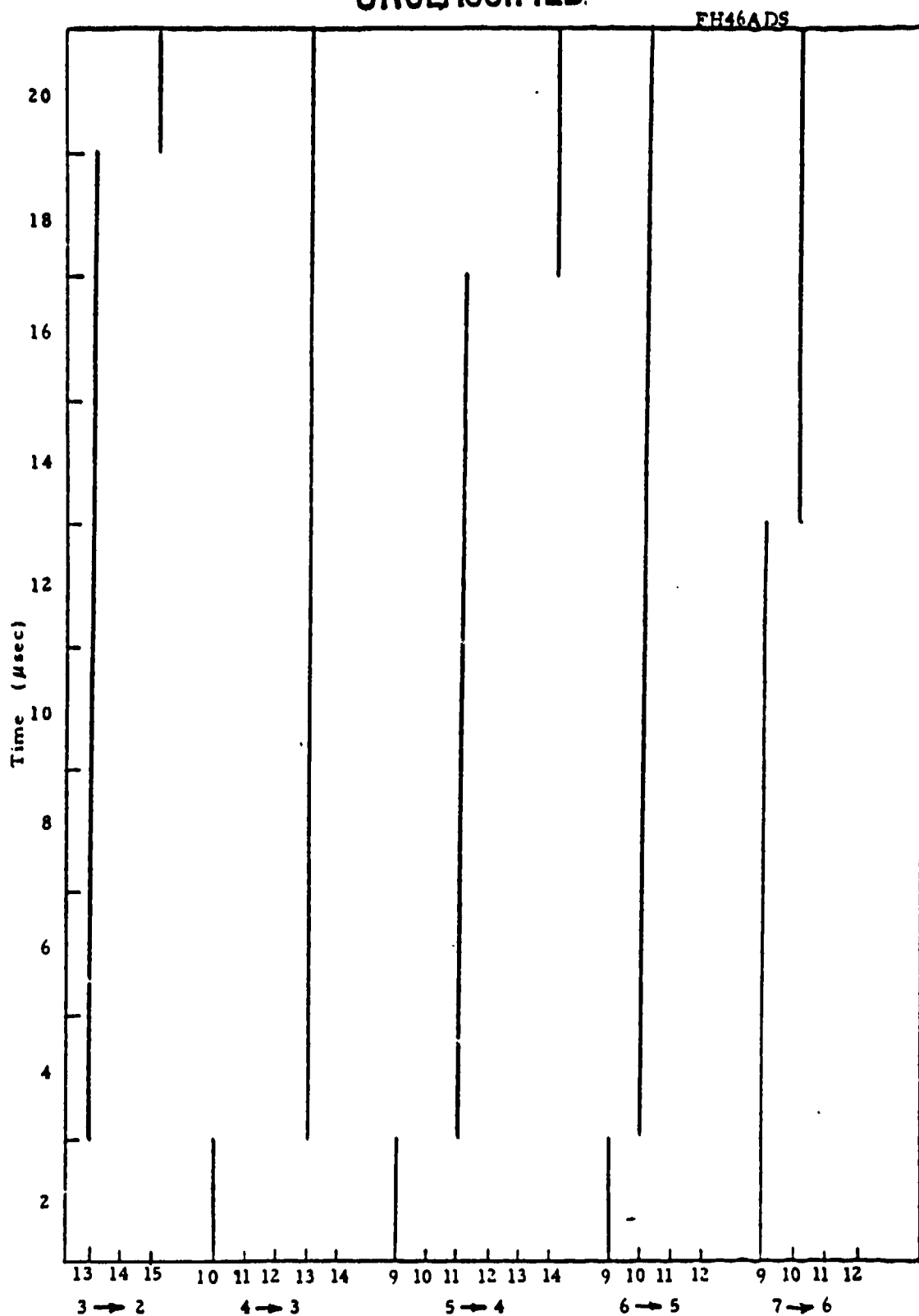
UNCLASSIFIED

FH61AM1



(U) Figure 2.16a Free running oscillator spectral output corresponding to Figure 2.14. (U)

UNCLASSIFIED

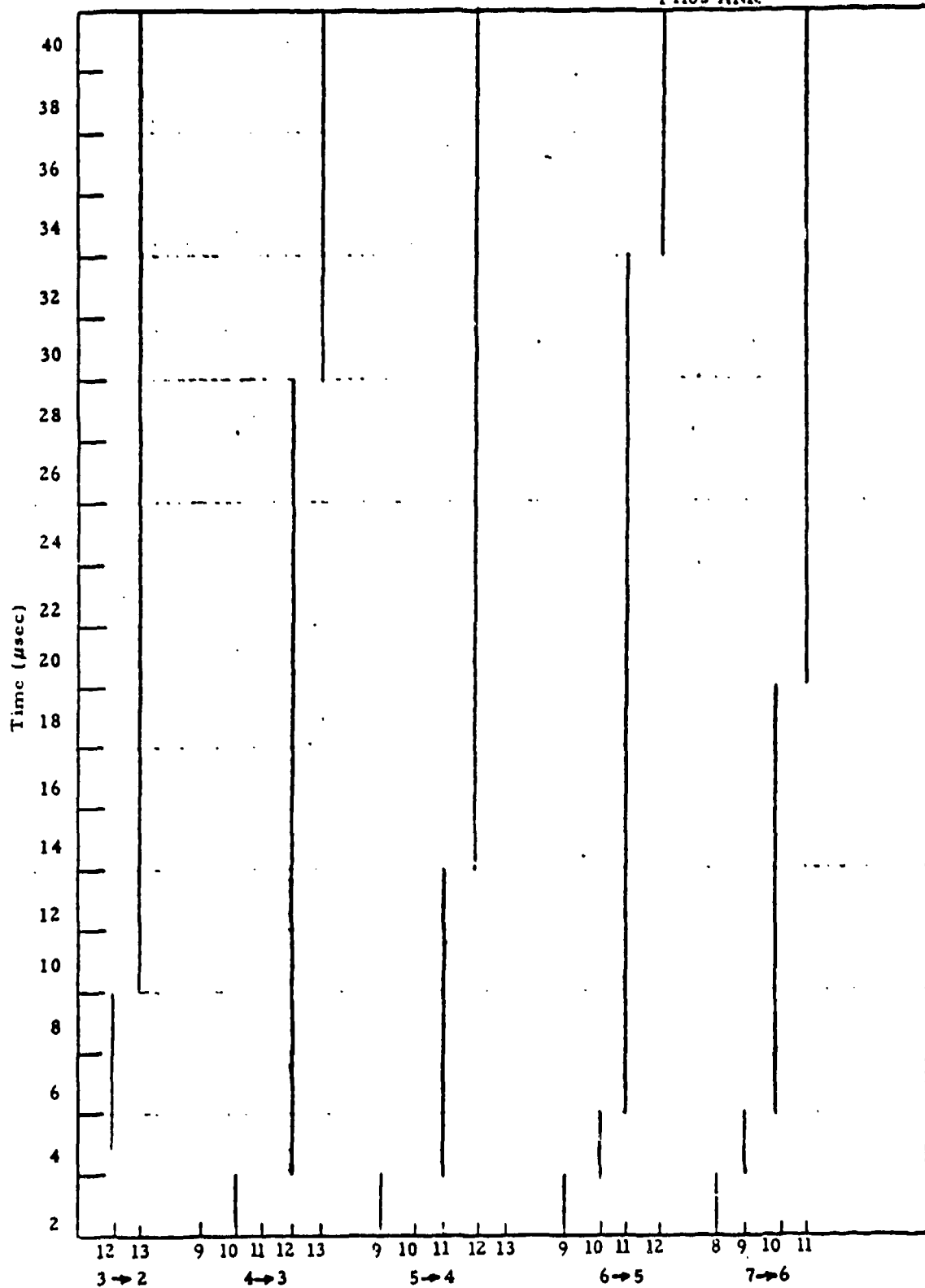


(U) Figure 2. 16b Line selected oscillator spectral output corresponding to Figure 2. 14. (U)

UNCLASSIFIED

UNCLASSIFIED

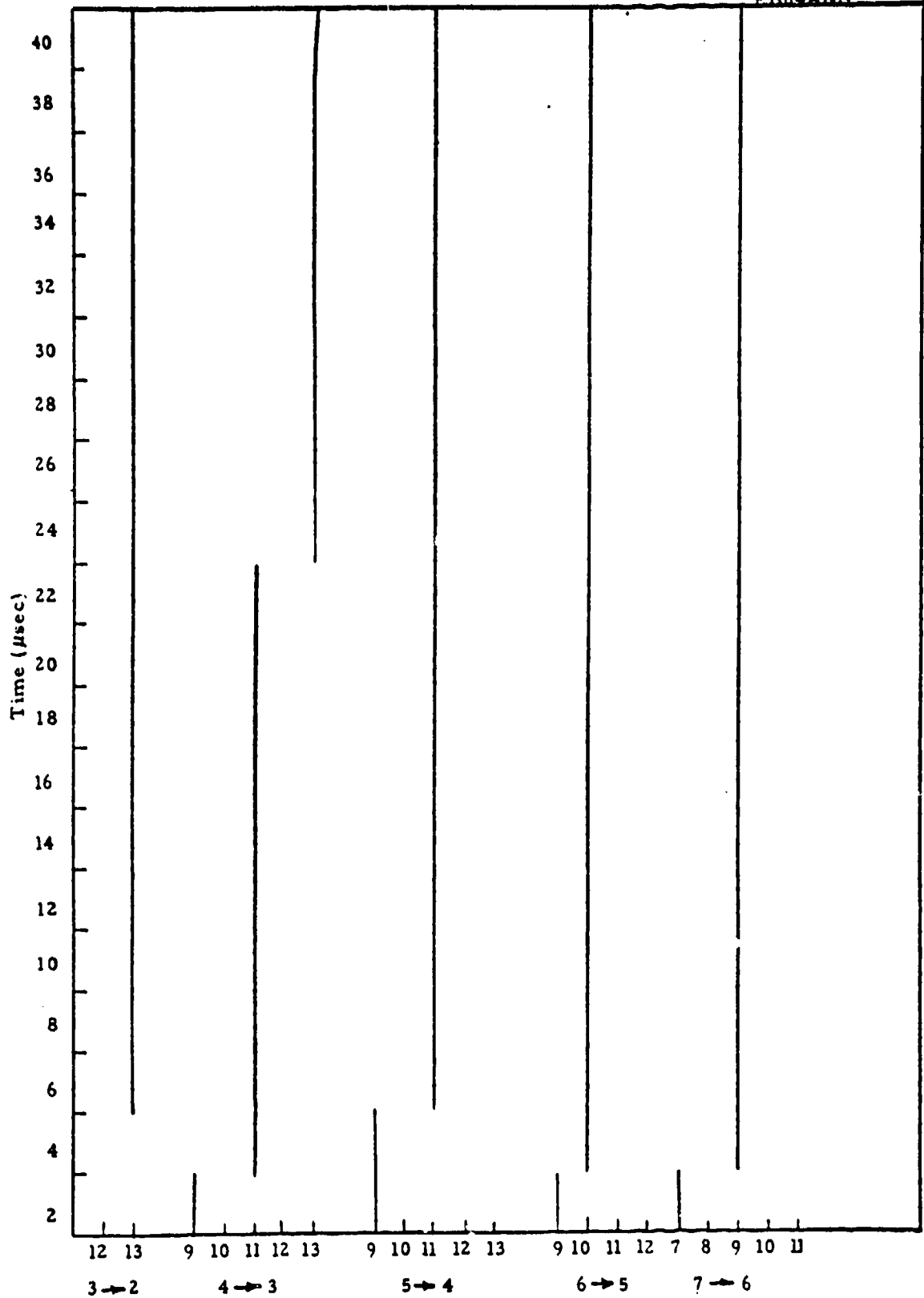
FH65 ANR



(U) Figure 2.17a Free running oscillator spectral output corresponding to Figure 2.15. (U)

UNCLASSIFIED

FH64ANH



(U) Figure 2.17b Line selected oscillator spectral output corresponding to Figure 2.15. (U)

UNCLASSIFIED

3.0 VV CROSS RELAXATION RATE

(U) A concerted effort has been made to obtain a VV rate matrix which would consistently fit both the transient and the steady state gain data reported in the previous quarterly report.² A more coherent set of VV rate values appear to be emerging from these efforts.⁴

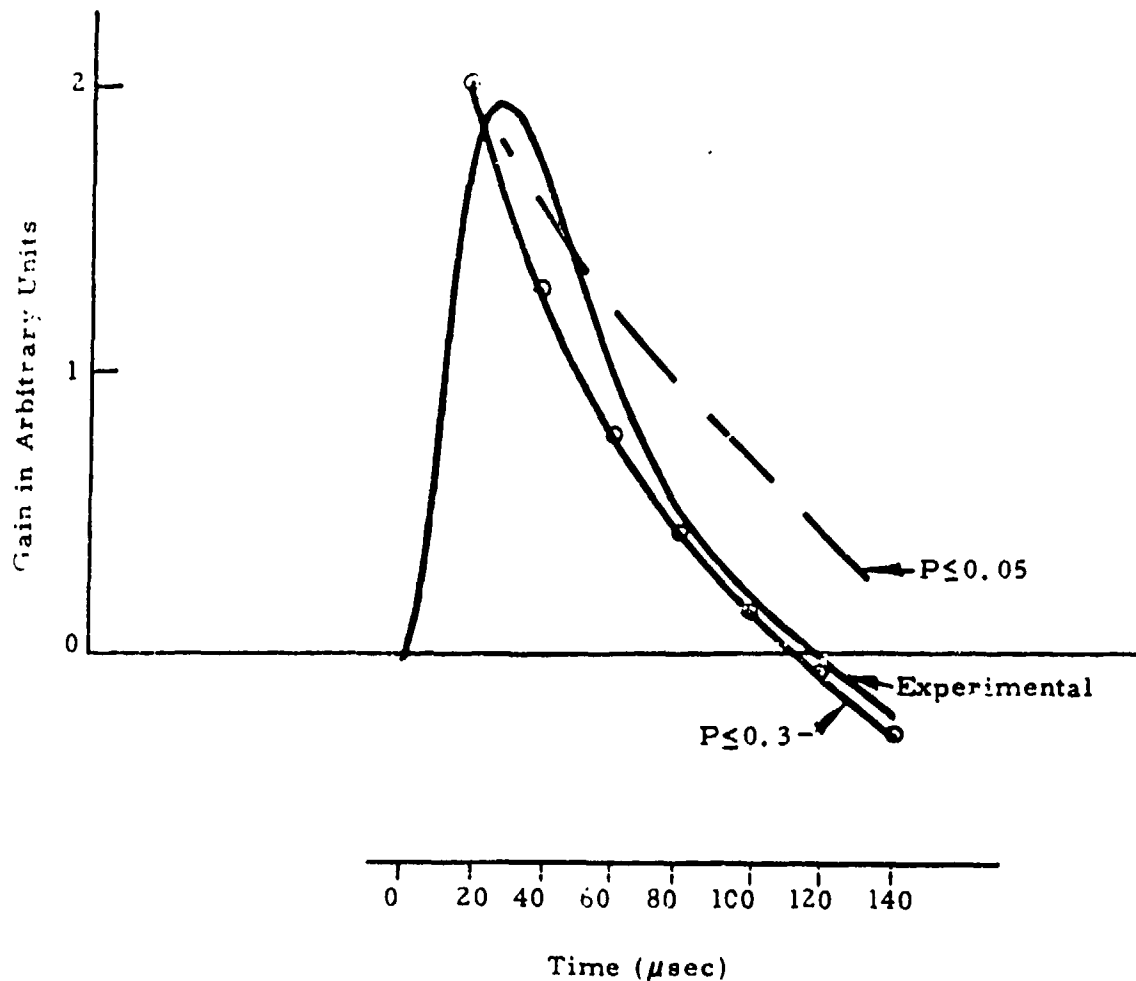
(U) It was reported earlier² that the probability of vibrational energy transfer per collision predicted by the Jeffers and Kelley theory³ had to be truncated somehow since probabilities become greater than unity for moderately high vibrational bands. The probability truncation deemed necessary to fit the steady state gain data was 0.01 while that needed to fit the transient gain data was ~ 1.0 . We now propose a resolution to this inconsistency.

(U) Kelley⁵ has postulated from theoretical analysis that the probability should be truncated at 0.3. The transient gain data fit quite well with this truncation as shown in Figure 3.1. It is also obvious from Figure 3.1 that truncation at a lower value, viz., 0.05 does not provide a good fit to the transient gain curve; truncation at 0.01, used in the previous report² to fit the steady state gain data, gives an even worse fit.

(U) At this point, it was suspected that the CO partial pressure measurements corresponding to the steady state gain data reported previously may not have been accurate. These pressures were measured by a variable reluctance electrical pressure gauge. A more absolute method is provided by calibrating the gas flow meter with actual collection of gas samples for a known period of time. The two methods indeed gave different values of the partial pressures under the same operating conditions. Since the method of pressure measurement by sample collection is more accurate, the partial pressures of CO were remeasured, and the correct values are shown in Table III below.

UNCLASSIFIED

(U) Figure 3.1 The experimental curve gives the time variation of gain for $V = 9 \rightarrow V = 8$ in the presence of a saturating pulse of 2.4 watts/cm^2 in the transition $V = 8 \rightarrow V = 7$. The curve labeled $P \leq 0.3$ shows the transient gain obtained by theoretical modeling with probability truncation at 0.3. The curve $P \leq 0.05$ is also obtained theoretically by probability truncation at 0.05. (U)



UNCLASSIFIED

(U) TABLE III. CO Partial Pressures in Torr (U)

<u>Previous Measurements</u>	<u>Corrected Measurements</u>
0.1	0.19
0.2	0.33
0.3	0.47
0.4	0.61

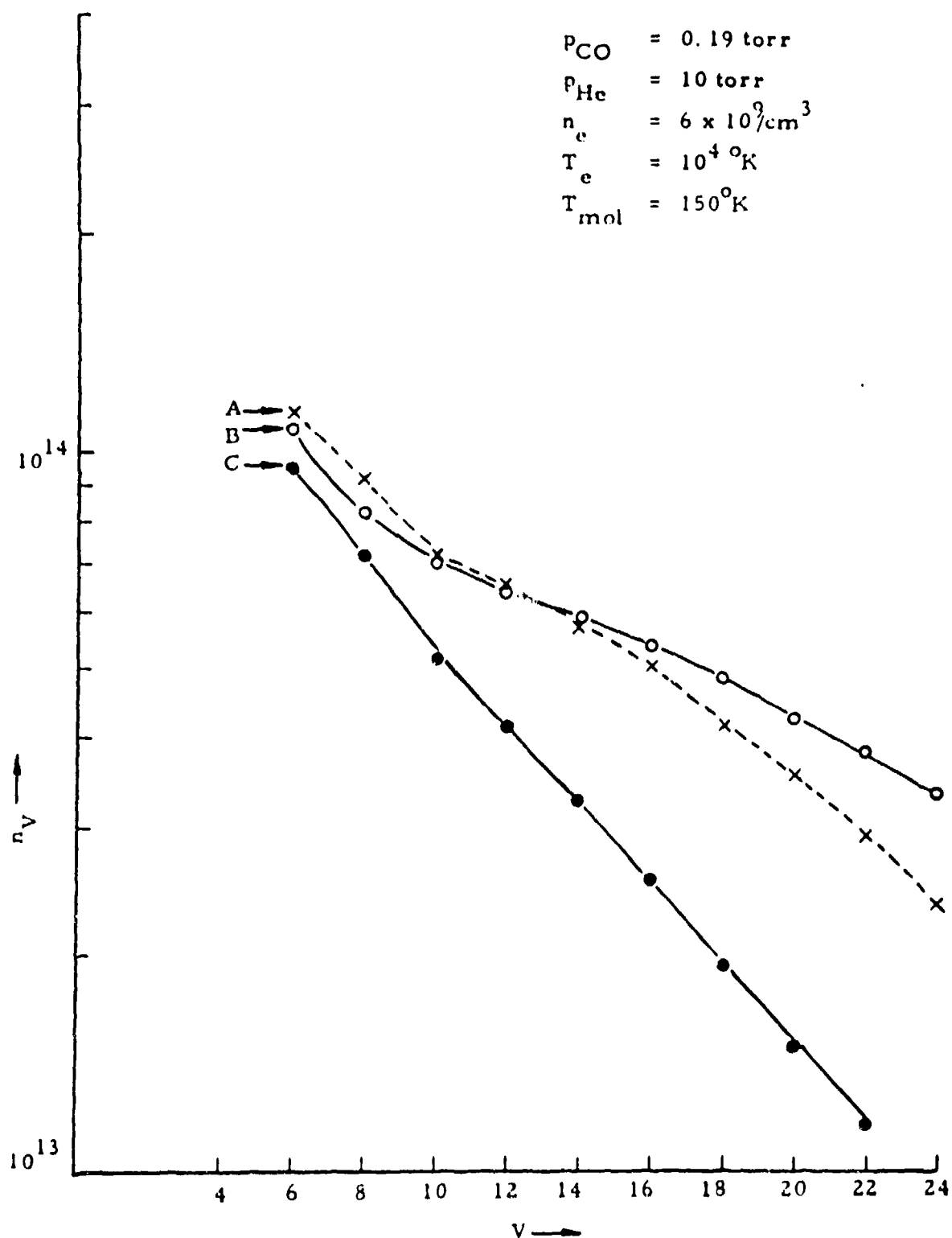
(U) Theoretical modeling to obtain the population density distribution was carried out with the corrected partial pressures and the probability truncation at 0.3. The results obtained for the 0.19 torr CO partial pressure case are shown in Figure 3.2 (Curve B). For comparison, the experimental population densities derived from gain measurements (reported earlier) are shown by Curve C. It is evident from the figure that the population densities obtained by theoretical modeling (Curve B) are much too high at the higher vibrational levels, as compared to the experimental population densities (Curve C).

(U) After careful examination of the different parameters, it was observed that the theoretical population density will be close to that obtained experimentally if the optical broadening cross section was assumed to be higher at the higher vibrational levels. The experimental population densities reported previously were derived from the steady state gain data with an optical broadening cross section that was assumed to be constant for all the v levels. This assumption was made in the absence of any reported data on how the broadening cross section of a diatomic molecule varies with the vibrational levels. However, measurements⁶ of broadening cross section for the CO fundamental vibrational band ($1 \rightarrow 0$) indicate that this cross section can differ by as much as a factor of 2 just from a change in the rotational quantum number. It would, therefore, be more appropriate to assume that the broadening cross section should

UNCLASSIFIED

UNCLASSIFIED

(1) Figure 3.2 Curve A and C give population densities obtained from gain measurements: C with constant optical broadening cross section, A with higher optical broadening cross sections at higher V level. Curve B gives the population densities obtained by theoretical modeling. (U)



UNCLASSIFIED

change with v levels as well. Intuitively it seems reasonable that an anharmonic molecule like CO may have a larger optical broadening cross section when it vibrates with a larger amplitude at a higher v level than at the ground vibrational level.

(U) Accordingly, a tentative functional dependence for the broadening cross section σ was assumed to be

$$\sigma_{v \rightarrow v-1} = \left[1 + \frac{v-1}{6} \right] \sigma_{1 \rightarrow 0}.$$

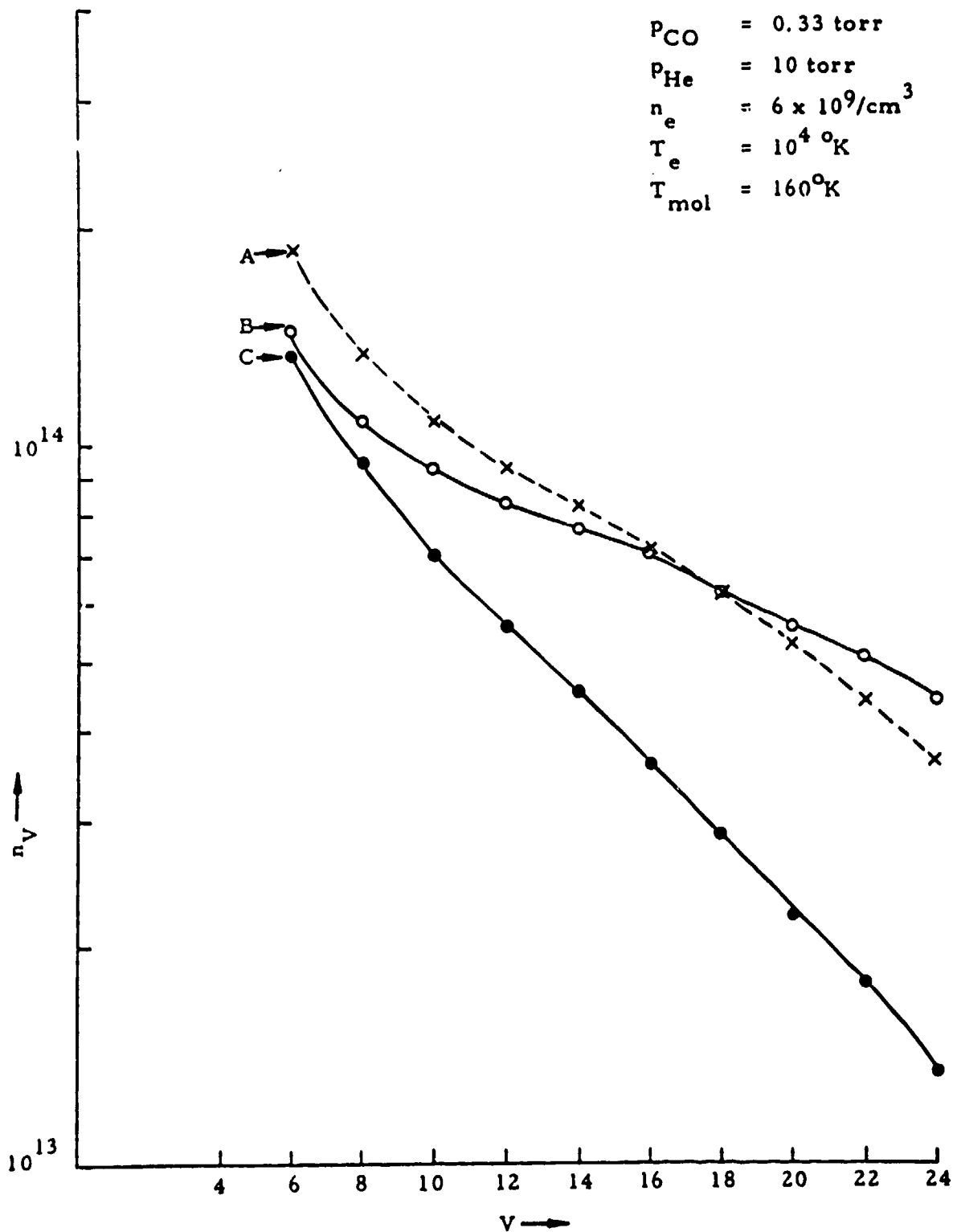
(U) The experimental population densities derived from the steady state gain data by using the above functional dependence of σ is shown in Figure 3.2 (Curve A). The closer agreement of this experimental population density with those obtained by theoretical modeling with the larger optical broadening cross section at higher v levels appears to support this assumption. A similar trend is exhibited by the data at CO partial pressures of 0.33 torr, 0.47 torr, and 0.61 torr shown respectively in Figures 3.3, 3.4 and 3.5.

(U) The above agreement is not exact, possibly due to one or more of the following factors:

1. The tentative functional dependence of σ may not be quite correct. The exact dependence should be determined experimentally.
2. Inclusion of deactivation by wall collision would change the theoretical population densities. At present there is no data to indicate how many vibrational quanta are lost by wall collisions, or the probabilities of deactivation per collision.

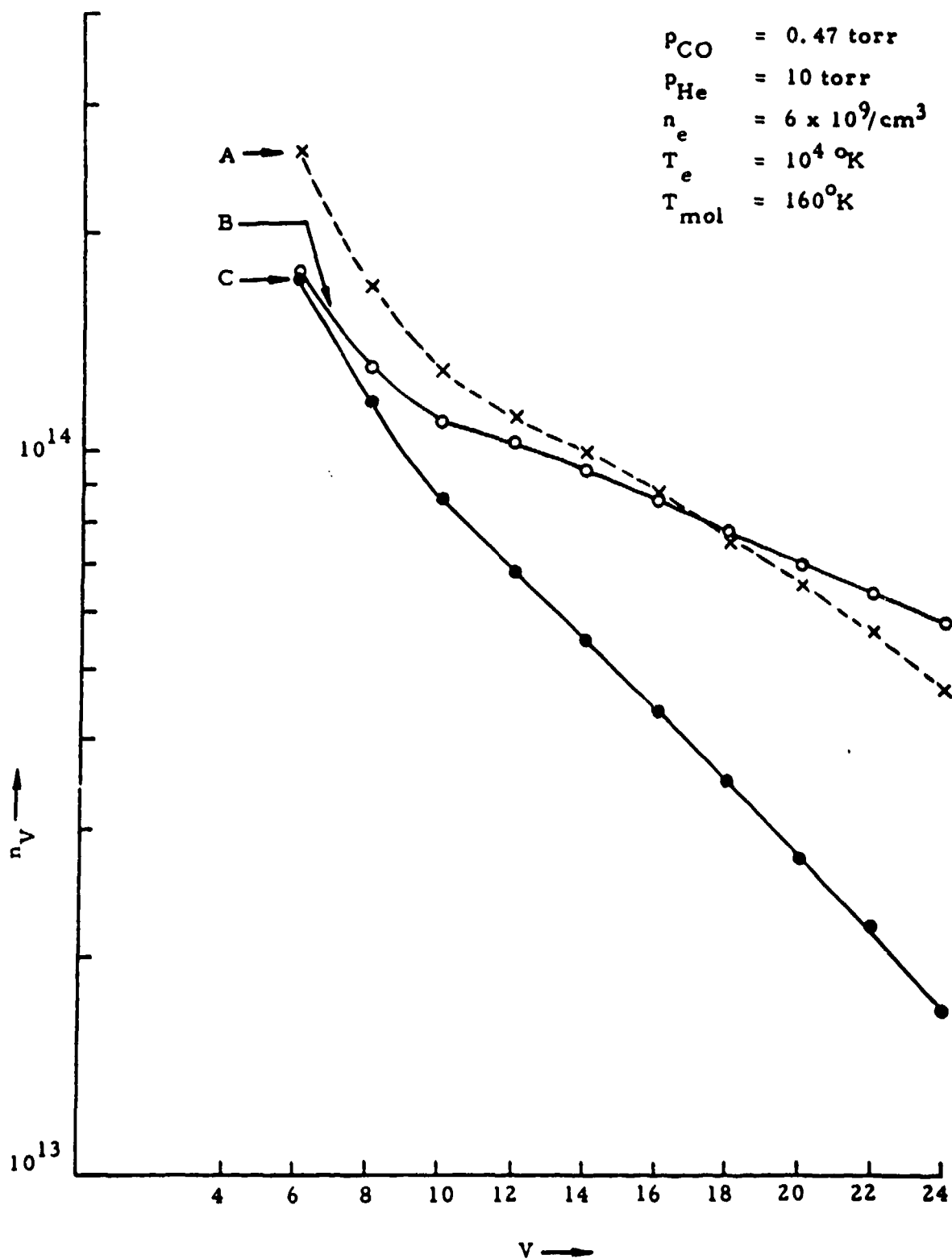
UNCLASSIFIED

(U) Figure 3.3 Curve A and C give population densities obtained from gain measurements: C with constant optical broadening cross section, A with higher cross section at higher V level. Curve B gives the population densities obtained by theoretical modeling. (U)



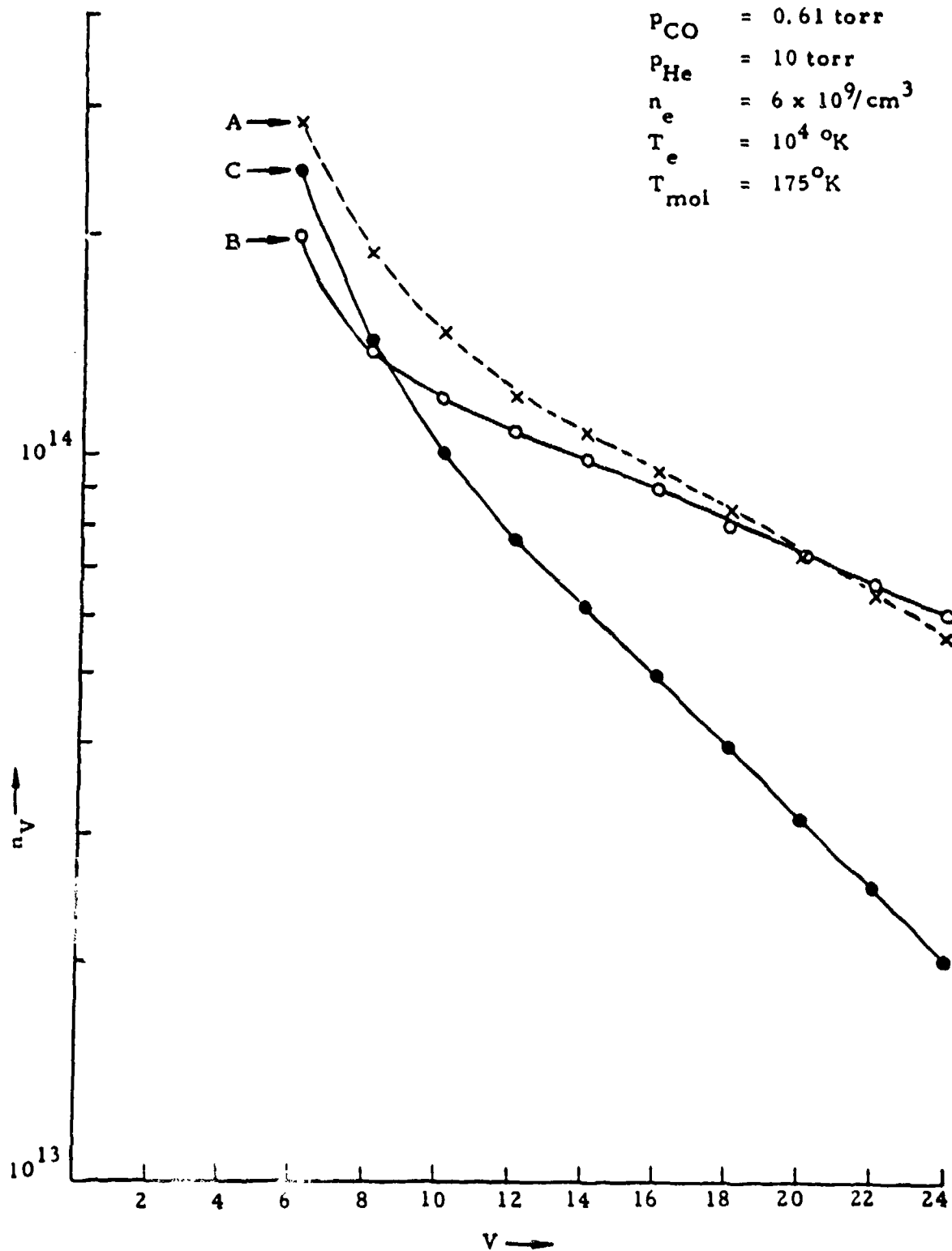
UNCLASSIFIED

(U) Figure 3.4 Curve A and C give population densities obtained from gain measurements: C with constant optical broadening cross section, A with higher cross section at higher V level. Curve B gives the population densities obtained by theoretical modeling. (U)



UNCLASSIFIED

(U) Figure 3.5 Curve A and C give population densities obtained from gain measurements: C with constant optical broadening cross section, A with higher cross section at higher V level. Curve B gives the population densities obtained by theoretical modeling. (U)



UNCLASSIFIED

3. VT rates may be higher at higher vibrational bands. There are some indications⁷ that this may be true since vibrational population of higher v levels, obtained by chemical reactions, seem to be deactivated equally irrespective of collision partners. However the effect of higher VT rates will change the populations only at higher v levels without any significant change in the low v levels.

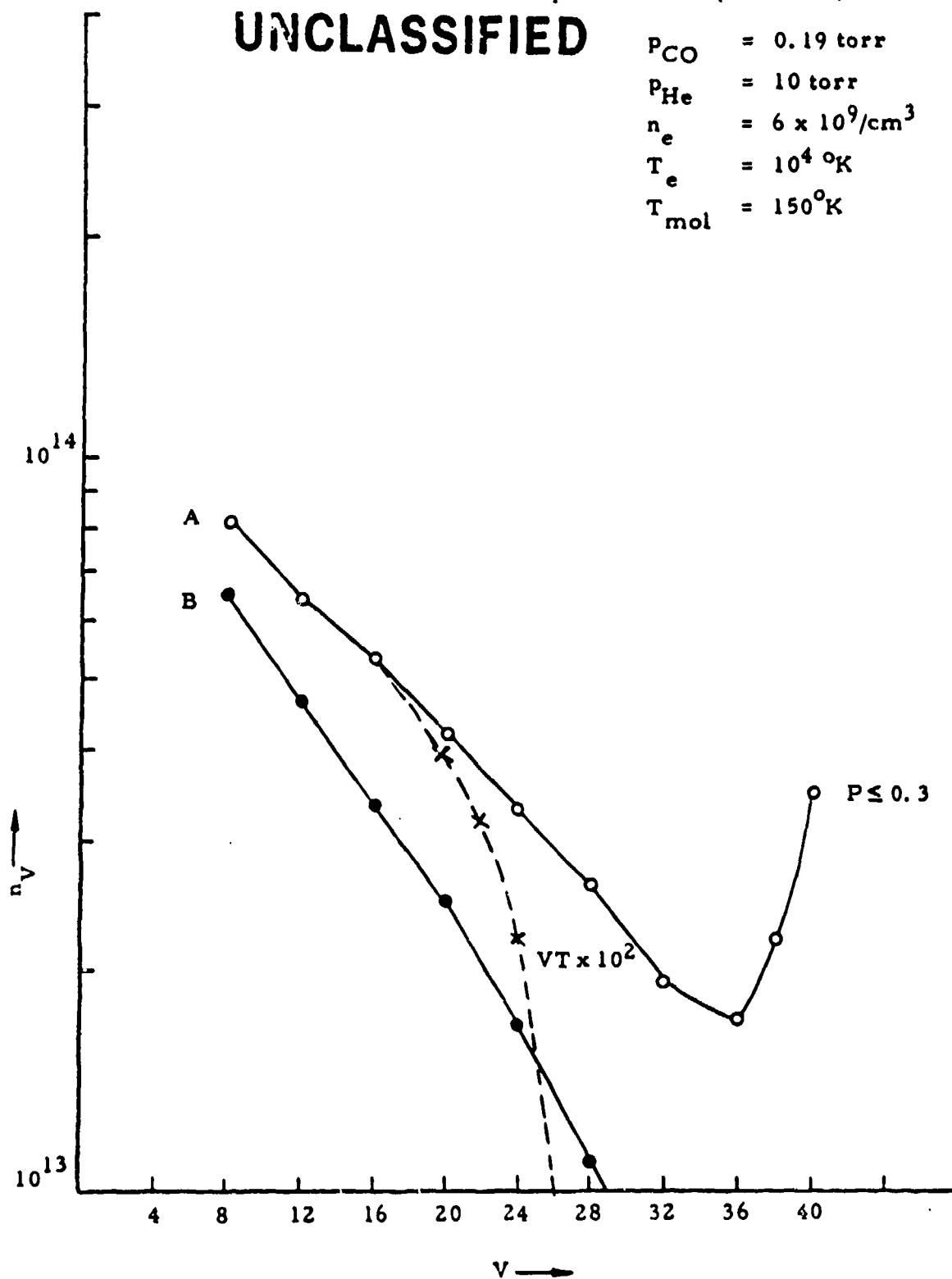
(U) Figure 3.6 illustrates some extreme cases of the factors listed above. Curve A gives the theoretical population densities for CO partial pressure of 0.19 torr. The dotted part of Curve A is obtained if the log of the VT rate is linearly increased to make the rate 100 times larger at $v = 40$. Curve B is obtained if wall collisions deactivate all quanta with a probability of 1 per collision at a rate determined by the time of diffusion from the center to the wall in a tube of 1 cm radius.

(U) Clearly the correct identification of VV rates cannot completely be resolved before more experiments are performed to determine the functional dependence of σ , effect of wall collisions and the magnitude of VT rates at higher v levels. However, from the analysis carried out so far, the rate matrix generated by including both long range and short range forces and truncating the probability per collision at ~ 0.3 appears to yield relatively consistent results with several experimental measurements over a significant range of parameters.^{1, 2, 4}

(U) Figure 3.6 Solid curve A gives the population densities obtained by theoretical modeling; the dotted part shows the effect of increasing VT rates to be 100 times larger at $V = 40$. Curve B gives the population densities under the same conditions as in solid curve A, but with the inclusion of wall deactivation of all quanta with a probability of 1. (U)

UNCLASSIFIED

$P_{CO} = 0.19 \text{ torr}$
 $P_{He} = 10 \text{ torr}$
 $n_e = 6 \times 10^9 / \text{cm}^3$
 $T_e = 10^4 \text{ }^\circ\text{K}$
 $T_{mol} = 150 \text{ }^\circ\text{K}$



UNCLASSIFIED

UNCLASSIFIED

4.0 E-BEAM LASER EXPERIMENTAL RESULTS

(U) The experimental configuration of the E-beam stabilized CO laser has been described previously, along with the results for various gas mixtures and pump powers.^{1,2,8} Results of some of the experimental parametric data are plotted in Section 2.0 where they are compared with theoretical calculations. As was indicated in the last report, the peak power and efficiency increase as the electrical pumping rate is increased, and CO/Ar mixtures appeared to give better results than CO/N₂ mixtures. Additional experimental evidence of this is shown in Figure 4.1. In all three photographs the top traces are the laser output intensity, the center traces are the total electron gun current, and the bottom traces are the sustainer current.

(U) Figure 4.1a, for a CO/N₂ mix, and 4.1b, for a CO/Ar mix, illustrate the results with peak pump powers of 1.0 kW/cm³. Threshold for the CO/N₂ mixture occurs much later than for the CO/Ar mixture and results in a lower energy output and lower efficiency. Note also the longer tail with the CO/N₂ mixture due to the transfer of excitation from N₂ to CO. Figure 4.1c is again a CO/N₂ mixture but the electrical pumping rate was increased to 2.1 kW/cm³. With this increased pump rate the threshold time, efficiency and energy output are all approximately equivalent to the result for the CO/Ar mixture shown in 4.1a.

4.1 Spectral Data. (U) Considerable effort has been expended to measure integrated and time resolved spectral characteristics of the E-beam device. The spectrum emitted from the laser needs to be identified for line selection investigations and is also required to provide insight about the gas kinetics and excitation processes. Time resolved spectral measurements have been

UNCLASSIFIED

TYPICAL EXPERIMENTAL RESULTS

P = 200 torr

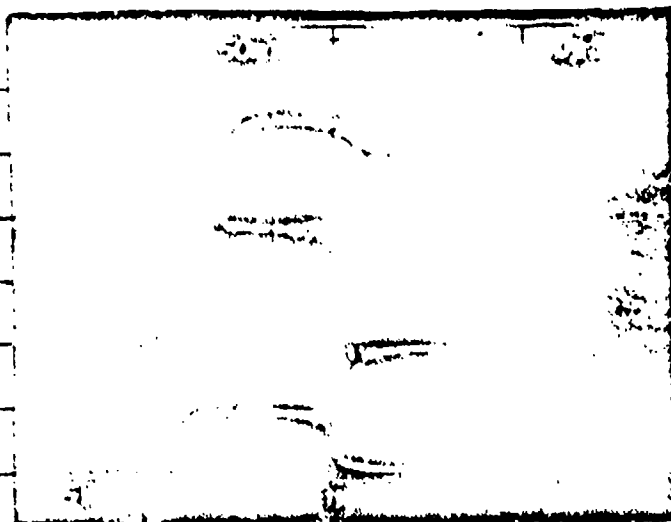
T = 150°K

UNCLASSIFIED

Detector

Gun Current
(2A/Div)

Sustainer
Current
(500A/Div)



CO:Ar 1:3

$P_{IN} = 1 \text{ kW/cm}^3$

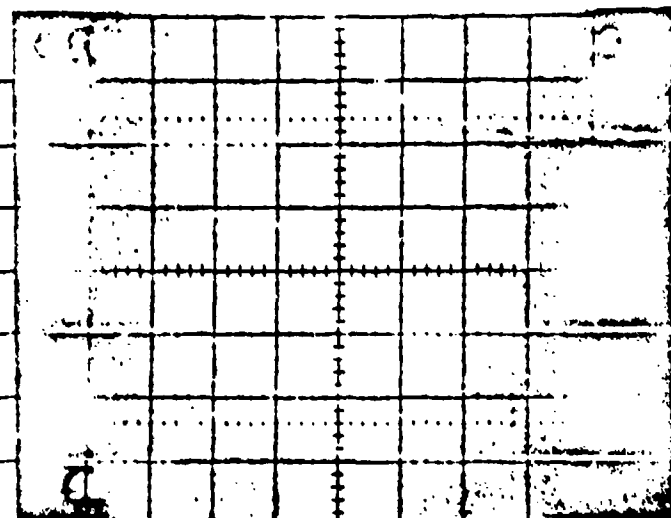
Output = 15 J

Conversion
Efficiency = ~25%

Detector

Gun Current
(2A/Div)

Sustainer
Current
(500A/Div)



CO:N₂ 1:4

$P_{IN} = 1 \text{ kW/cm}^3$

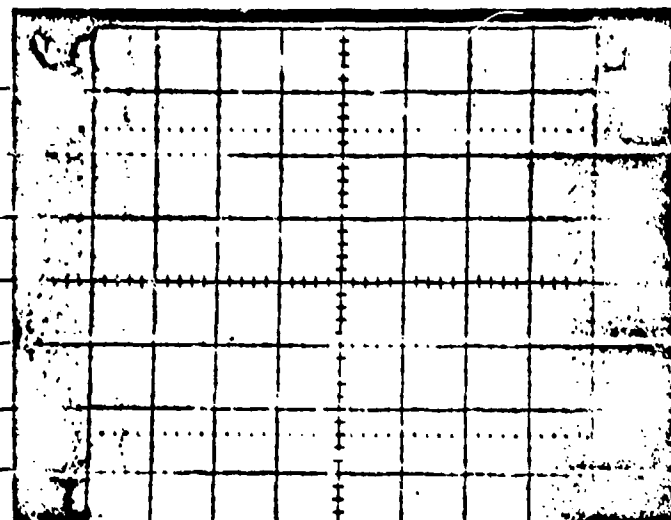
Output = 6.5 J

Conversion
Efficiency = ~10%

Detector

Gun Current
(2A/Div)

Sustainer
Current
(500A/Div)



CO:N₂ 1:4

$P_{IN} = 2.1 \text{ kW/cm}^3$

Output = 33 J

Conversion
Efficiency = ~25%

(U) Figure 4.1 Typical experimental results illustrating the effect of gas mixtures and electrical pumping rates on the laser output. (U)

UNCLASSIFIED

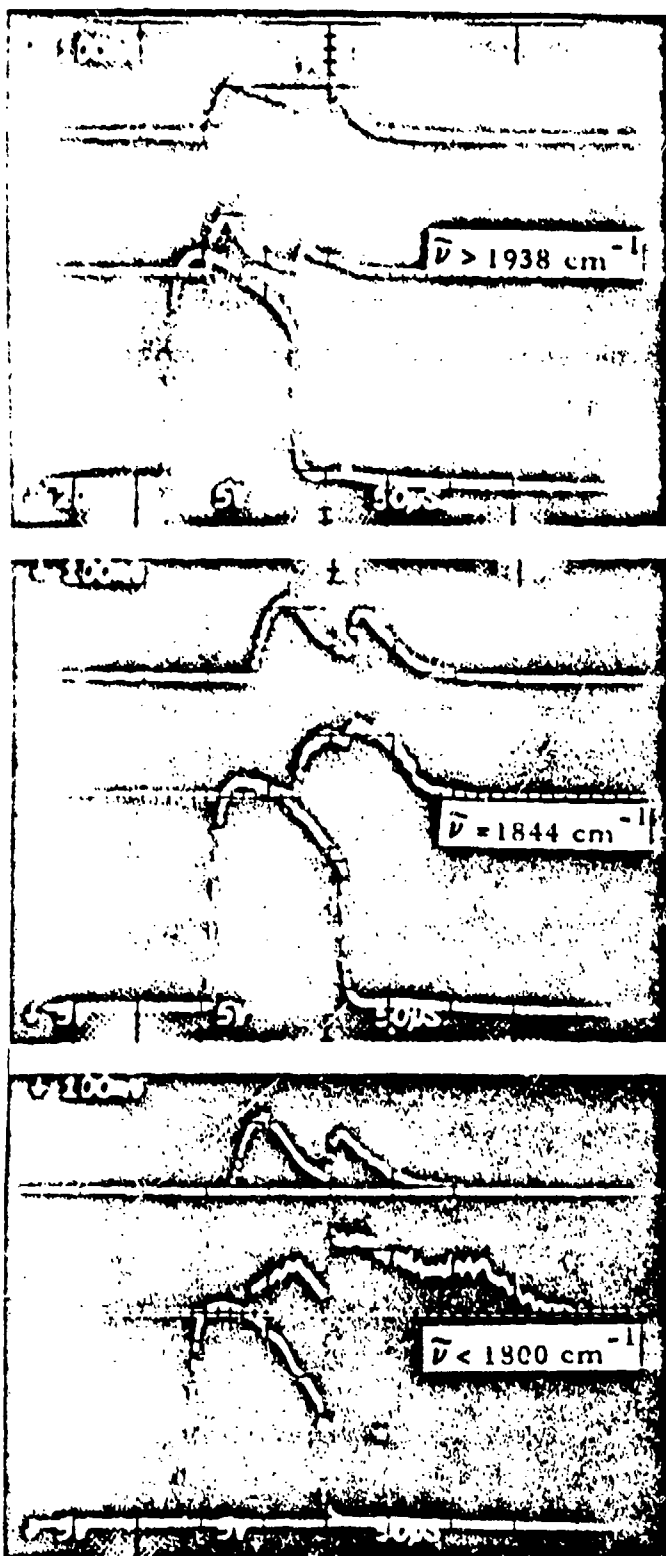
UNCLASSIFIED

made by placing an AuGe detector at the output of an optical engineering spectrometer. Typical results are illustrated in Figure 4.2. In each photograph the top trace is the spectrally integrated laser output, the center trace is the spectrometer output at the indicated wave number and the lower trace is the sustainer current. The general trend for all gas mixtures and pump rates studied was the same (most are low pump rates). The lowest vibrational bands reached threshold first and then turned off quickly. The "middle" vibrational bands turned on somewhat later but otherwise resembled the integrated trace. Finally, the after pulse consisted almost entirely of the higher vibrational bands. The range of bands emitted shifted downward with increased electrical pumping but the trend just described was always observed. In the example illustrated, Figure 4.2a shows the output from all bands 6-5 and below obtained by placing the detector behind a diffuser intercepting these lines. Figure 4.2b is the output from the transition 10-9P(17) and Figure 4.2c is the output from all bands 12-11 and higher.

(U) Shifting of the emitted bands with time appears to be a result of competition between the direct electrical excitation of the lower levels and excitation of the higher levels by VV pumping. However, the same result could occur if the heating rate was much greater than the rate indicated from theoretical predictions (typically 10% or less). For this reason, an experiment was set up to measure the gas temperature as a function of time by observing the fluorescence from nitrogen excited by an electron beam. Preliminary experiments at 300°K indicate that the temperature can be measured quite accurately and that the heating is not excessive. These experiments will be carried out more thoroughly at the cryogenic temperatures where the device is normally operated.

UNCLASSIFIED

TIME RESOLVED SPECTRA



$$P_{IN} = 3.5 \text{ kW/cm}^2$$

$$P_{CO} = 30 \text{ torr}$$

$$P_{Ar} = 85 \text{ torr}$$

$$P_{N_2} = 85 \text{ torr}$$

$$P_{TOT} = 200 \text{ torr}$$

$$T = 175^\circ\text{K}$$

(U) Figure 4.2 Time-resolved comparison of various spectral bands (central trace on each photograph) with the spectrally integrated output (upper traces). (U)

UNCLASSIFIED

UNCLASSIFIED

4.2 Device Development. (U) Problems with window seals and flow inhomogeneities in the nominal one liter device have limited experiments to temperatures of approximately 150°K and pressures of ~ 300 torr. To alleviate these problems, a new cooling jacket was constructed and modifications were made to the anode to improve flow uniformity. Failure of a cryogenic valve during initial testing of these changes resulted in considerable damage to the structure, necessitating rework which is presently in progress. Modifications have also been made to the gun to increase output current density and eliminate the possibility of loss of bias due to gun sparks.

The 10 liter device is nearing completion. The laser plenum is in final assembly. The heat exchanger for the laser gas has been constructed and tested. Temperature stability of approximately 0.1°C was attained which is well within the experimental requirements. Medium homogeneity measurements will begin shortly. The 10×100 cm area cathode gun has been successfully tested for vacuum integrity and the diagnostic equipment for uniformity measurements has been completed. Hot tests of the gun will commence shortly.

UNCLASSIFIED

UNCLASSIFIED

5.0 AREA CATHODE E-GUN DEVELOPMENT

(U) All of the major subassembly components of the area cathode E-gun have been completed, and initial testing of these components has commenced. A test program has been established to test the vacuum integrity, the high voltage isolation and the E-beam performance parameters of the design. The present projected schedule indicates that final E-gun testing should occur during the first half of November.

5.1 Experimental Tests. (U) Leak testing of the E-gun vacuum chamber has begun. Although pumping will be by an ion pump during normal E-gun operation, the preliminary pump down and helium leak testing is being done with a 4" diffusion pump utility system. A helium leak detector is being utilized to ensure that all of the heliarc welded joints and the O-ring seal on the E-beam window are leak tight.

(U) Helium leak probing of the E-gun vacuum envelope in the low 10^{-5} torr region indicates that the window O-ring seal, the heliarc welded joints and the metal gasketed flanges are all leak free. This testing was performed with a 12 mil thick window foil which will now be replaced with a 1 mil thick foil; the foil planned for use during E-gun operation.

(U) Upon completion of the vacuum tests, the high voltage components, which include the high voltage feedthrough, the support ceramics and the cathode-control grid shroud, will be installed for the purpose of high voltage testing. The system will be evaluated for corona and breakdown points.

(U) After the vacuum and high voltage integrity of the system has been established, the impregnated cathodes will be activated and the electron beam performance parameters will be evaluated. Of primary interest will be the current density and the current uniformity. The E-beam tests are

UNCLASSIFIED

also expected to establish the performance parameters of current versus bias voltage control, voltage droop, window scatter and window thermal loading.

5.2 Theoretical Calculations of Electron Transport Processes. (U) As part of the ongoing effort to evaluate the E-gun laser cavity system, two computer programs have been developed to calculate the effects of the window and gas scatter upon the primary electron beam profile as it penetrates the laser cavity. These calculations to date have confirmed qualitative observations of E-beam scatter observed in the one liter device. The program will be refined and applied to the 10 liter device so as to evaluate ionization density, sustainer field uniformity and lasing medium energy deposition.

(U) The electron beam experiences many small angle-small energy loss collisions with the window and gas electrons as it is slowed down. Because of the large interaction cross section, or short mean free path, the E-beam experiences an average divergence of 25° when passing through the E-gun window foil. The laser gas, although less dense, is thicker in the same proportion so that it contributes a comparable amount of scatter.

(U) The scatter distribution from the pencil beam experiment can be approximated quite well by a Gaussian function, because of the many small angle scatters,

$$f(\theta) = \frac{1}{\sqrt{2\pi} \bar{\theta}} \exp(-\theta^2 / 2 \bar{\theta}^2)$$

UNCLASSIFIED

where $\bar{\theta}$ is the average width of the scatter distribution which comes from experimental or theoretical results. One convenient empirical relation which correlates well with experimental data is⁹

$$\bar{\theta} = 56.6^\circ (d/R_o)^{1/3}$$

where

R_o = electron range in mg/cm^2

d = scatterer thickness in mg/cm^2

Typical values of $\bar{\theta}$ for 250 keV electrons are

$\bar{\theta} = 25^\circ$ for 1 mil Ti foil window

$\bar{\theta} = 15^\circ$ for 1 cm of N_2/CO gas at 1 atm and 100°K

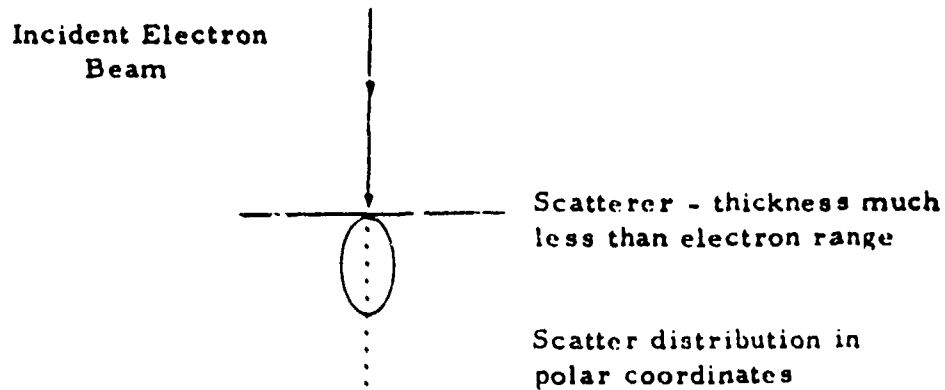
(U) The model used to calculate the primary E-beam spread resulting from foil and gas scatter is illustrated in Figure 5.1. The width of the beam has been divided into increments, Δx wide, which are then treated as pencil beams. The scatter distribution at the elevation Δy away from the scatter plane is obtained by summing the scatter contribution at each Δx of the new plane from all of the Δx 's of the previous plane.

5.3 Primary E-Beam Profile. (U) On the vacuum side of the E-gun window the current distribution is assumed to be flat over the entire beam width. This is illustrated by the curve marked O in Figure 5.2 which is the normalized primary beam current plotted as a function of the transverse position across the laser cavity. At a distance of 1 cm into the cavity, the primary current density profile is illustrated by curve #1. The roll-off at the beam edges is a result of the window scatter, which is uniform

UNCLASSIFIED

ELECTRON BEAM DIVERGENCE ANALYSIS

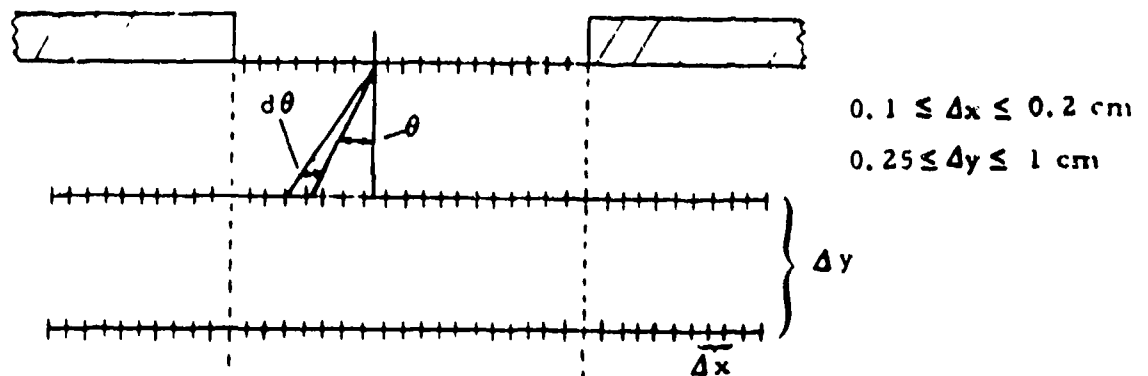
A) ELECTRON SCATTER DISTRIBUTION:



Scatter Distribution Function: $f(\theta) = \frac{1}{\sqrt{2\pi} \bar{\theta}} \exp(-\theta^2 / 2 \bar{\theta}^2)$
(Gaussian)

$\bar{\theta}$ = Average width of scatter distribution which comes from experimental and theoretical results

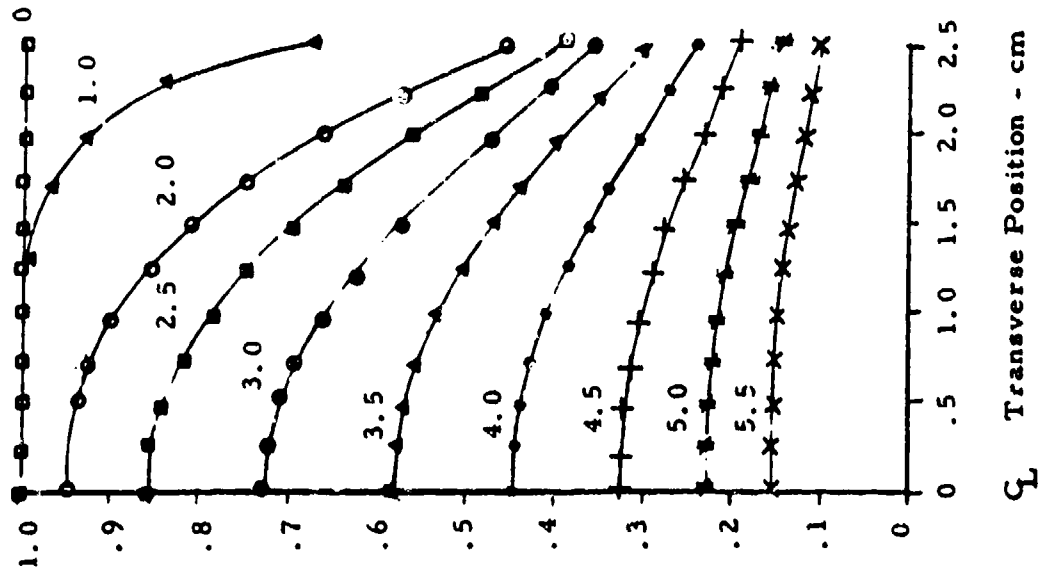
B) WINDOW AND GAS SCATTER MODEL:



(U) Figure 5.1 Window and Gas Scatter Model (U)

UNCLASSIFIED

DEVICE #1
150 keV Electrons
100°K Gas
760 torr



(U) Figure 5.2 E-Beam Current Distribution in Laser Cavity (U)

UNCLASSIFIED

over the entire area. The center scatter is compensated for by scatter from the Δx 's adjacent to the center so that the centerline intensity is not affected at the 1 cm level. At successively greater distances into the laser cavity the primary beam intensity is diminished by continued scatter, with the resultant effect as illustrated in Figure 5.2.

(U) The laser cavity geometry used for the calculated primary E-beam profiles of Figure 5.2 is the present one liter device. The configuration is typical of E-beam stabilized lasers in that there is scatter from the window, the gas layer between the window and the laser cavity, and the cavity itself.

5.4 Cavity Electric Field. (U) From the primary E-beam intensity and profile data of Figure 5.2, it is possible to calculate the sustainer power supply electric field across the height of the cavity. Because of electron-ion recombination within the laser gas, the ionized gas charge carrier density is proportional to the square root of the primary E-beam current density.

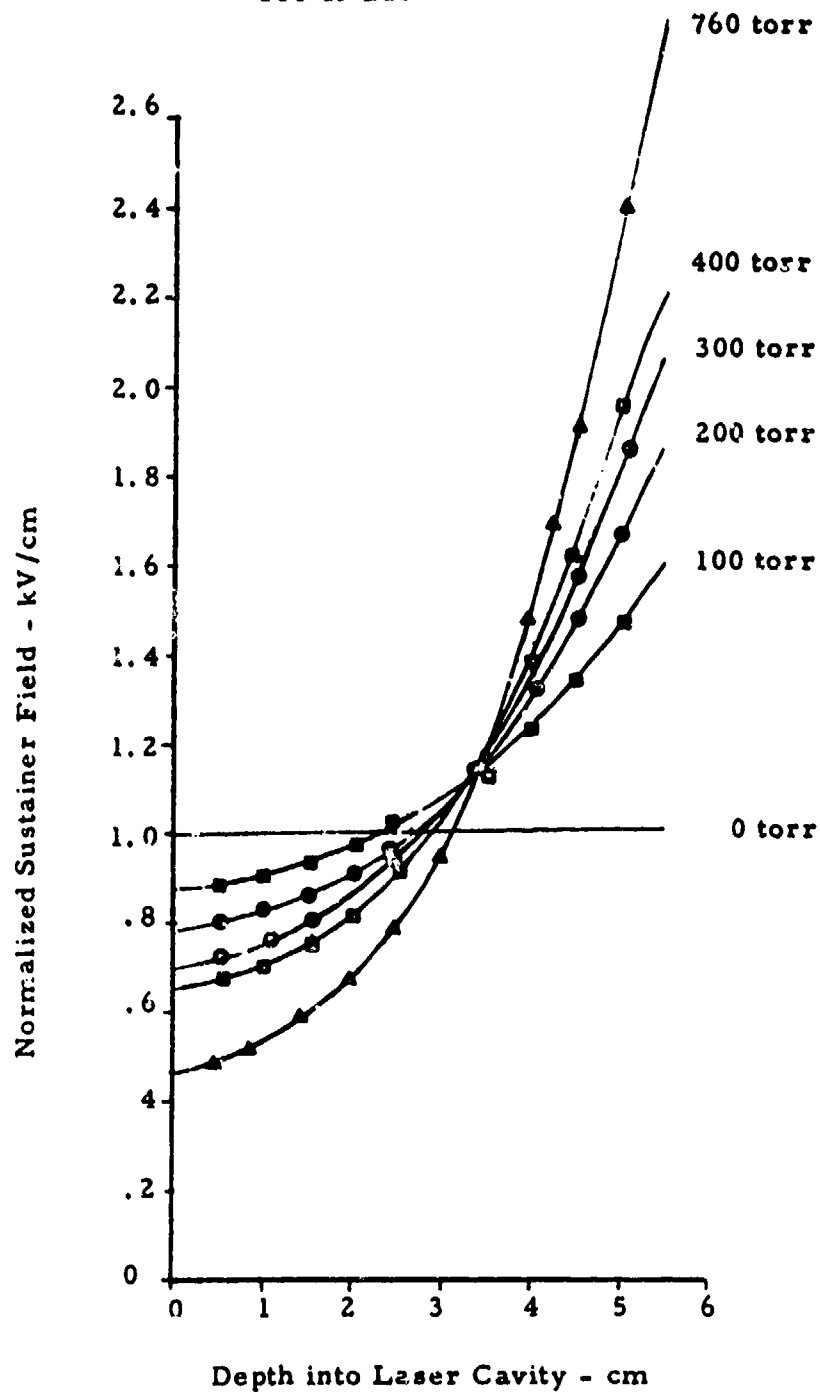
(U) Initial calculations of the laser cavity sustainer electric field were made using an average primary E-beam current intensity at each distance in the cavity (the average over the entire width of the cavity at that distance). This is an approximation which does not take into account the variation in primary E-beam intensity across the width of the cavity, but it does yield quantitative results.

(U) The data plotted in Figure 5.3 is the sustainer field at increasing depths into the laser cavity. The sustainer field is normalized to be 1 kV/cm for uniform ionization. Deviations from the 1 kV/cm field result from the window and gas primary electron beam scatter. At the top of the cavity where the beam density is high, the gas ionization is also high so that the medium cannot support as high a field at the bottom where the ionization is less.

UNCLASSIFIED

DEVICE #1

150 keV Electrons
100°K Gas



(U) Figure 5.3 Laser Cavity Sustainer Field (U)

UNCLASSIFIED

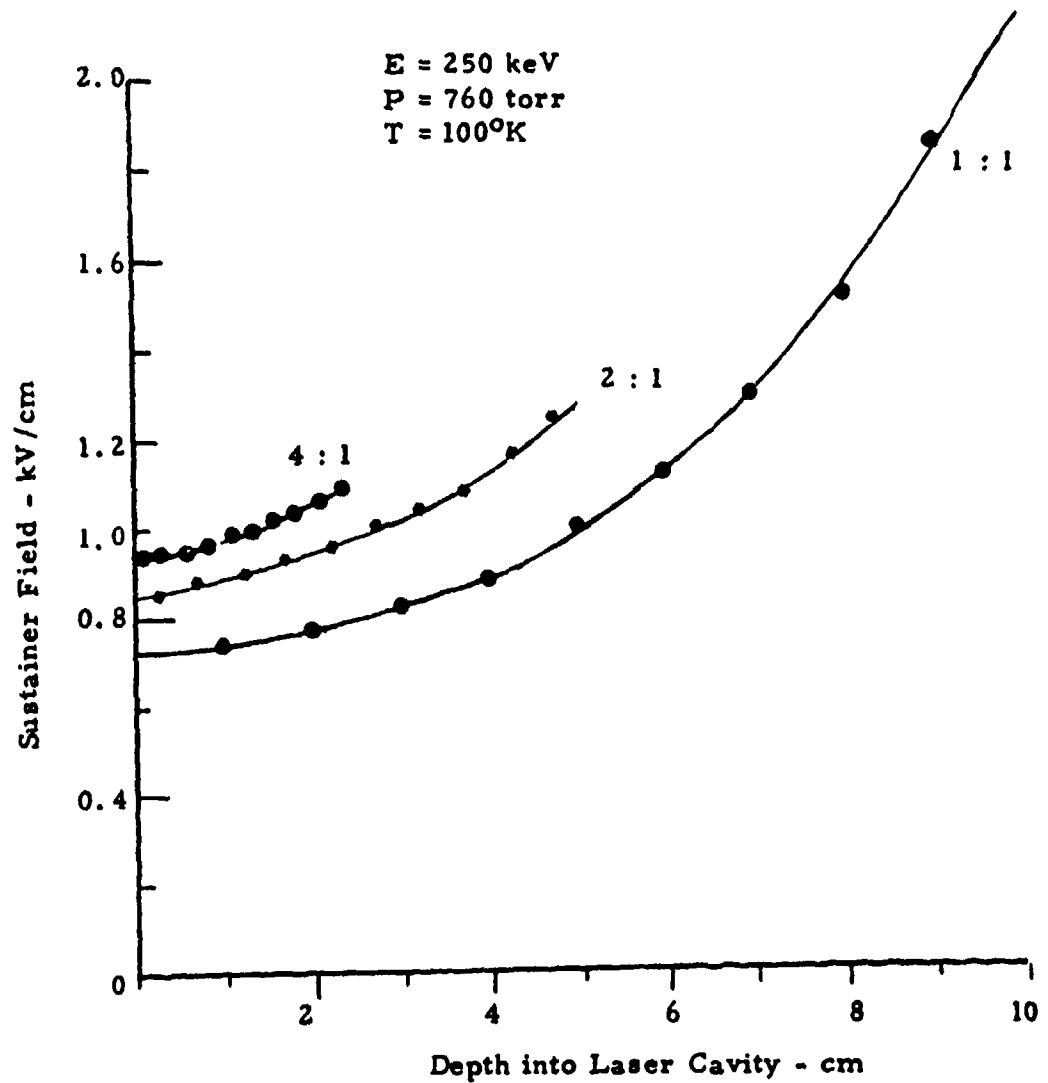
(U) A program is being developed at the present time to treat the ionized gas of the laser cavity as a resistance network. This should yield more accurate calculations of the gas ionization density, the sustainer field distribution, and the sustainer energy deposition.

5.5 Cavity Aspect Ratio. (U) The amount of E-beam scatter out of the laser cavity is determined in large part by the cavity aspect ratio, the ratio of the width to the height. The results discussed were for a cavity of aspect ratio 1. By making the cavity width larger than its depth, the electron scatter loss area, as a proportion of the cavity surface area, is reduced. The effect is a more uniform ionization and thus more uniform distribution.

(U) The results of calculations for laser cavities of varying aspect ratios are illustrated in Figure 5.4. Here it can be seen that ratios of even 2:1 yield suitable field uniformities.

UNCLASSIFIED

SUSTAINER FIELD VARIATION FOR CAVITIES
OF DIFFERENT ASPECT RATIOS



(U) Figure 5.4 Sustainer Field Uniformity (U)

55
UNCLASSIFIED

UNCLASSIFIED

c 0 REFERENCES (U)

1. W. B. Lacina, "Transient Oscillator Analysis for a CO Laser," to be presented at 25th Gaseous Electronics Conference, London, Ontario, October 17-20, 1972.
2. Northrop Report NLSD72-14R, Third Quarterly Technical Status Report, High Power CO Laser, July 1972.
3. W. J. Jeffers and J. D. Kelley, J. Chem. Phys. 55, 4433 (1971).
4. M. L. Bhaumik, W. B. Lacina and M. M. Mann, "Vibrational Relaxation in CO Lasers," to be presented at 25th Gaseous Electronics Conference, London, Ontario, October 17-20, 1972.
5. J. D. Kelley, "Vibrational Energy Transfer Processes in Collisions between Diatomic Molecules," (to be published).
6. J. P. Bouanich and C. Haeusler, J. Quant. Spectrosc. Radiant. Transfer 12, 695, 1972.
7. R. C. Millikan (private communications).
8. G. McAllister, M. M. Mann, R. G. Eguchi and G. Hasserjian, "High Power Electron Beam - Stabilized CO Laser," to be presented at 25th Gaseous Electronics Conference, October 17-20, 1972, London, Ontario.
9. Baranov and Pavolovskii, "Passage of Electrons through Matter," Atomnaya Energiya 25, 317, 1968.

Security Classification

DOCUMENT CONTROL DATA - R & D

(Security classification of title, body of abstract and indexing annotation must be entered when the overall report is classified)

1. ORIGINATING ACTIVITY (Corporate author) Northrop Corporation, Northrop Research and Technology Center, Laser Technology Laboratories		20. REPORT SECURITY CLASSIFICATION SECRET - NO FORN	
3. REPORT TITLE Fourth Quarterly Technical Status Report, High Power CO Laser (U)		20. GROUP	
4. DESCRIPTIVE NOTES (Type of report and inclusive dates) Fourth Quarterly Technical Status Report, June through August 1972			
5. AUTHOR(S) (First name, middle initial, last name) Laser Technology Laboratories			
6. REPORT DATE September 1972		7A. TOTAL NO. OF PAGES 56	7B. NO. OF REFS 9
8A. CONTRACT OR GRANT NO. N00014-72-C-0043		8B. ORIGINATOR'S REPORT NUMBER(S) NRTC 72-10R	
8. PROJECT NO.		9B. OTHER REPORT NO(S) (Any other numbers that may be assigned this report) none	
10. DISTRIBUTION STATEMENT (In addition, security equipment which must be marked this document is subject to special export controls and such transmittal to foreign governments or foreign nationals may be made only with prior approval of Office of Naval Research (Code 421), Arlington, Virginia 22217.)			
11. SUPPLEMENTARY NOTES None		12. SPONSORING MILITARY ACTIVITY Advanced Research Projects Agency, ARPA Order No. 1806	
13. ABSTRACT (U) The fourth quarter effort on the High Power CO Laser Program is reviewed. The program is directed toward the development of the required CO laser technology, the required component technology and the design and construction of intermediate power laser devices. The results of analytical and experimental investigation of the basic characteristics of the laser and data from a high pressure electrically excited CO laser device are discussed.			

DD FORM 1473
1 NOV 66

Security Classification

KEY WORDS	LINK A		LINK B		LINK C	
	ROLE	WT	ROLE	WT	ROLE	WT
CO Laser Molecular Lasers Electrical Discharge Lasers High Power Lasers						



DEPARTMENT OF THE NAVY
OFFICE OF NAVAL RESEARCH
800 NORTH QUINCY STREET
ARLINGTON, VA 22217-5660

IN REPLY REFER TO

5510/6
Ser 93/891
8 Oct 98

From: Chief of Naval Research
To: Administrator
Defense Technical Information Center
ATTN: William Bush, DTIC-OCQ
8725 John J. Kingman Road Suite 0944
Ft. Belvoir, VA 22060-6218

Subj: CHANGE OF DISTRIBUTION STATEMENT

1. Permission is granted to change the distribution statement for the following documents to
Distribution Statement A: Approved for Public Release; Distribution is Unlimited:

AD 527 922⁶
AD 523 538¹

2. Questions may be directed to the undersigned on (703) 696-4619.

A handwritten signature in black ink, appearing to read "Peggy Lambert", is positioned above the printed name.

PEGGY LAMBERT
By direction